Towards Sustainable Satellite Swarms

MSc Aerospace Engineering Thesis

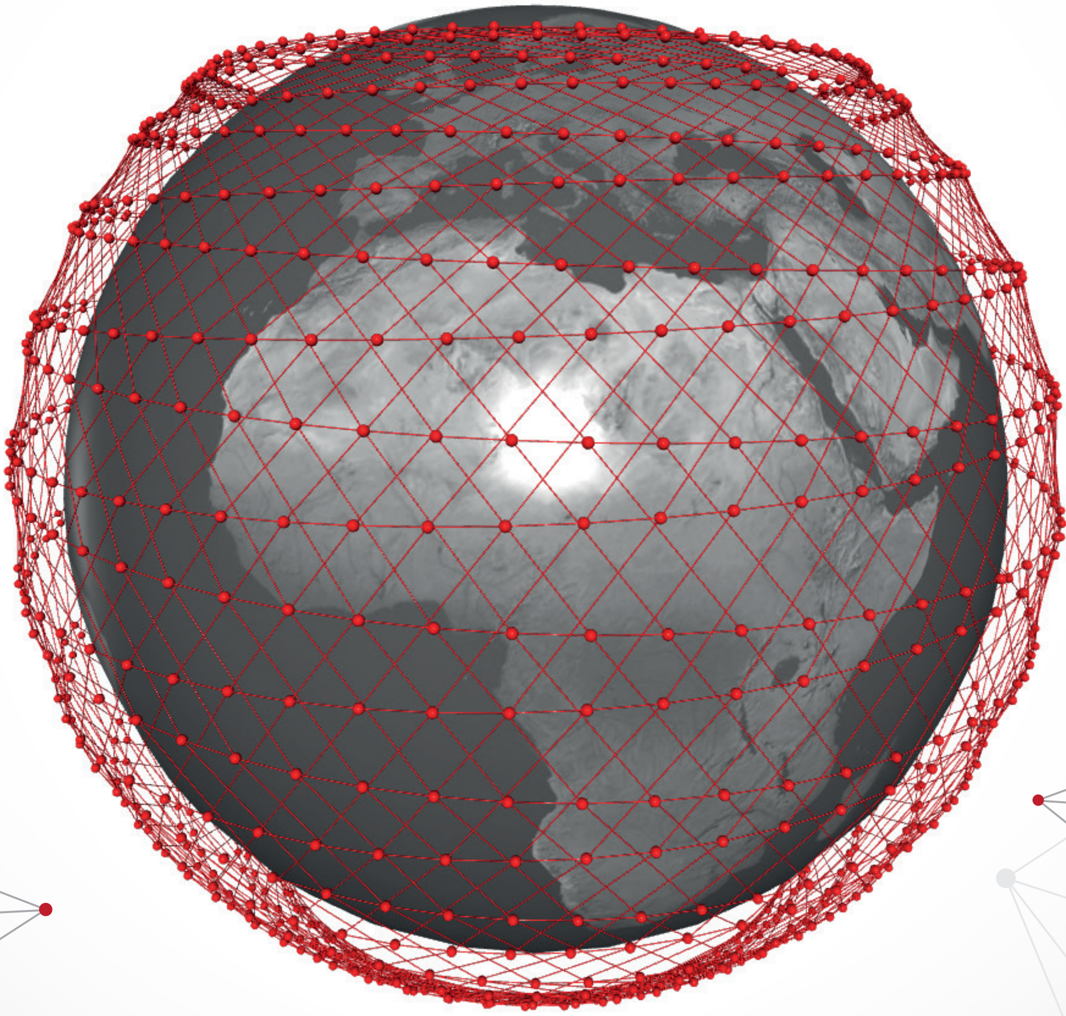

Calum Turner

isae
Institut Supérieur de l'Aéronautique et de l'Espace
SUPAERO

TUDelft

Towards Sustainable Satellite Swarms

Presented in partial fulfilment of the requirements of a Master of Science in Aerospace Engineering, Space Systems track

Author:
Calum Turner

Supervisors:
Dr. Raj Thilak Rajan
Prof. Dr. Stéphanie Lizy-Destrez

Starting date of the internship:
April 15th 2021

Duration of the internship:
6 months

Due date of the report: November 19th 2021
Submission date: November 19, 2021

Declaration of Authenticity

This assignment presents my own work under the guidance of Dr. Raj Thilak Rajan. Literature and other sources are properly indicated with appropriate citations in the text. All sources of information used in this piece of work are properly cited and are included in the bibliography. The figures in this thesis are my own work or are cited appropriately. I understand that plagiarism constitutes serious academic misconduct and may result in disciplinary action being taken.

Date: November 19, 2021

Acknowledgements

This work was conducted at TU Delft and was partly supported by the Dutch-PIPP (Partnerships for Space Instruments & Applications Preparatory Programme), funded by NWO (Netherlands Organisation for Scientific Research) and NSO (Netherlands Space Office).

This work makes use of data available at the CGEE CubeSat database [1] as well as the software packages Astropy[2], a community-developed core Python package for Astronomy [1], [2] and Poliastro[3], a community-developed astrodynamics package [3]. This thesis also makes partial use of latex code prepared by Paolo Guardabasso, a PhD student at ISAE-SUPAERO, which is gratefully used with permission.

There are several people I would like to thank for their support during my internship at TU Delft. Dr. Rajan at TU Delft has been endlessly supportive and informative as I grappled with unfamiliar topics and ideas. Thank you for your guidance and for supporting my academic curiosity, as well as trusting me to research new and unexpected topics. The comments, feedback and suggestions of the Circuits and Systems group at TU Delft were also helpful and their insights informed large parts of this thesis. The support of dr. Stéphanie Lizy-Destrez at ISAE-SUPAERO is also very much appreciated.

I am deeply grateful to my friends and family, without whose personal and practical support I would not have completed this thesis or my degree as a whole.

Finally, and most importantly, I am grateful for the support, feedback, and companionship of my wife, who made living in the Netherlands incalculably more fun and without whom this thesis would not have been possible.

[1] https://www.cgee.org.br/web/observatorio-espacial/bancos-de-dados
[2] http://www.astropy.org
[3] https://www.poliastro.space

Abstract

Satellite swarms are an emerging mission architecture which offer a flexible, robust alternative to traditional space missions. Drawing inspiration from naturally occurring swarms such as honey bees or ant colonies, satellite swarms consist of individual satellite agents working cooperatively towards a common goal. Distributed multi-agent space systems are, however, inherently problematic from the point of view of space sustainability. Given the increasingly likely prospect of operational satellite swarms, and considering that mitigating the build up of space debris is necessary to preserve our access to space and space-enabled services, the question of how to sustainably operate satellite swarms requires answering. This report presents two projects to explore how satellite swarms could be made more sustainable.

In the first project we explored cooperative localisation in a satellite swarm. Using the well-studied Starlink satellite internet mega-constellation as a model swarm, we established the potential performance of cooperative localisation between 1584 Starlink satellites and 87 ground stations by calculating the Cramér-Rao Bound (CRB) at 573 simulated time steps. Our results show that the average Root Mean Square Error for localising the Starlink satellites has a constant value of approximately 10.15 m and varies between a maximum of 36.5 m and a minimum of around 2m. This result is determined primarily by the geometry of the Starlink mega-constellation and the characteristics of the inter satellite links, and gives values comparable to GNSS hardware currently on satellites. The values are also in agreement with previous research.

In the second project, we introduce a satellite health indicator, a composite indicator capturing the health of a swarm satellite. We also present ongoing research modelling swarm satellites with Markov chains using CubeSat subsystems as a basis for the subsystems of swarm satellites. We also present an analysis of historical CubeSat failures using data from the CGEE CubeSat database, which shows that 18.1% of all CubeSats launched currently present a risk to space sustainability.

We conclude both projects with a discussion of next steps and future research in these emerging topics.

Keywords: Satellite Swarms, Space Sustainability, Cooperative Localisation, Satellite Health Monitoring

Contents

List of Figures

List of Tables

Acronyms

+Grid Plus Grid

ADCS Attitude Determination and Control System

ADR Active Debris Removal

AOA Angle-Of-Arrival

CAS Circuits and Systems

COTS Commercial Off-The-Shelf

CRB Cramér–Rao Bound

ESA the European Space Agency

FCC Federal Communications Commission

GCRS Geocentric Celestial Reference System

GEO Geostationary Earth Orbit

GNC Guidance, Navigation, and Control

GNSS Global Navigation Satellite System

IAC International Astronautical Congress

ISAE-SUPAERO Institut Supérieur de l'Aéronautique et de l'Espace

ISL Inter-Satellite Link

ISLs Inter-Satellite Links

LEO Low Earth Orbit

LOS Line Of Sight

OBDH On-Board Data Handling

RMS Root Mean Square

RMSE Root Mean Square Error

RSOs Resident Space Objects

RSS Received-Signal-Strength

SSA Space Situational Awareness

STM Space Traffic Management

TOA Time-Of-Arrival

TTC Telemetry, Tracking, and Command

TU Delft Technische Universiteit Delft

UN COPUOS United Nations' Committee on the Peaceful Uses of Outer Space

Chapter 1

Introduction

This report presents the results of a 6-month internship completed in partial fulfilment of the requirements of a MSc in Aerospace Engineering at Institut Supérieur de l'Aéronautique et de l'Espace (ISAE-SUPAERO). During this project, I investigated the topic of space sustainability and satellite swarms at Technische Universiteit Delft (TU Delft), aiming to find a way to bring satellite swarms into alignment with the philosophy of space sustainability.

Space sustainability encompasses the set of methods, technologies, and regulations which ensure that humanity can enjoy continued access to space now and in the future without compromising the space environment with the build-up of debris or the overcrowding of operational satellites. At present, rising launch rates, satellite collisions, debris, and even anti-satellite weapon tests threaten sustainable operations in space.

Two projects are presented in this thesis, covering two very different aspects of satellite swarms and space sustainability. The first explored cooperative localisation in satellite swarms, aiming to determine if the interconnected nature of swarm satellites could provide a redundant method of localising satellites on orbit. The second project laid the groundwork for autonomous health monitoring in satellite swarms by developing a composite indicator to capture the health of the swarm satellite, modelled on CubeSat subsystems. This thesis focuses mainly on determining the potential of cooperative localisation in satellite swarms, though the preliminary investigations and results of the autonomous health monitoring project are also presented.

This report is structured as follows: some context regarding the working situation at TU Delft is presented in Chapter 2. Chapter 3 provides the background and motivation for this thesis, describing satellite swarms and space sustainability. Chapter 4 presents the larger research project, investigating the limits of cooperative localisation in a satellite swarm using Starlink as a case study. Chapter 5 presents preliminary research into autonomous satellite health monitoring in satellite swarms. Finally, conclusions are drawn from the research and personal reflections on the challenges and opportunities of the internship are presented in Chapter 6. Various supplementary appendices are provided at the end of the report.

Chapter 2

Work Context

2.1 TU Delft

TU Delft is the oldest and largest public technological university in the Netherlands, and was founded in 1842. It is one of Europe's leading technical universities and provides Bachelors, Master's and PhD degrees in a range of disciplines. Its researchers work in a variety of engineering fields and work to apply science and mathematics to solve practical problems affecting society and industry. In the field of space engineering, TU Delft's Space Institute investigates Sensing from Space, Space Robotics, and Distributed Space Systems. The university has also built and launched a 3U CubeSat, Delfi C^3.

2.2 The Circuits and Systems Group at TU Delft

This internship was conducted in the Circuits and Systems (CAS) research group at TU Delft, under the supervision of Assistant Professor Dr. R.T. Rajan[1]. The CAS group focuses on the theory and applications of signal processing, including high-level digital system design.

The research areas of this group include audio and acoustics, wireless communication, radio astronomy, distributed sensing from space, biomedical signal and image processing, and sensor fusion as well as investigating distributed systems such as satellite swarms. The CAS research group approaches problems by creating a sound mathematical framework for the analysis of problems from design to implementation.

2.3 Working Structure

Due the evolving Coronavirus restrictions in the Netherlands, I spent the majority of the internship working remotely with weekly meetings with Dr. Rajan alternating between online and in person meetings in Delft. As this internship was unfunded I worked 80% time at TU Delft, with the reaming 20% of the working week spent working as a freelance science writer[2]. As well as regular meetings with Dr. Rajan, I attended the seminars of the CAS group and presented updates on my work.

[1] Dr. Rajan's biography and publication record can be found at this link.

[2] More information on my science writing can be found here.

I worked autonomously through the week, researching papers or writing code and developing the methodology presented in this report. Dr. Rajan supervised my work and provided guidance and insight during our weekly meetings, as well as feedback on written material and interim results. We stayed in contact via email and communicated via Zoom and a shared GitHub repository where the documentation and code for this research project was stored.

As the coronavirus restrictions became less severe in the Netherlands, I was able to visit TU Delft up to four times per week, as well as access IT services, digital journals, and the library. This also facilitated more spontaneous discussions with my colleagues at CAS and led to new lines of investigation.

2.4 Previous Work

This research follows a summer internship during 2020 at TU Delft, which was conducted mostly remotely due to the COVID-19 pandemic. The 2020 summer internship culminated in the paper *"End-of-Life for Satellite Swarms"*, which was presented at the 71^{st} International Astronautical Congress (IAC) [4]. In that paper we suggested a swarm satellite health indicator, which combines various factors to provide a convenient metric to state and predict the 'health' of a swarm satellite. This swarm satellite health indicator was the first step towards answering one of the primary research questions of this internship: how should we deal with the tension between satellite swarms and space sustainability? The core concept of the satellite health indicator proposed in *"End-of-Life for Satellite Swarms"* is presented in detail in Section 5.1.

Chapter 3

Background & Motivation

3.1 Satellite Swarms

Satellite swarms are an emerging mission architecture which offer a flexible, robust alternative to traditional space missions. Drawing inspiration from naturally occurring swarms such as honey bees or ant colonies, satellite swarms consist of individual satellite agents working cooperatively towards a common goal. Despite efforts to classify distributed satellite systems [5], there is as yet no agreed-upon definition of a satellite swarm. For this thesis, we used a working definition of a satellite swarm as *a network of intercommunicating satellites exhibiting complex emergent behaviour, collectively operating as a distributed system* [6][7].

Complex emergent behaviour — which distinguishes satellite swarms from satellite constellations — is the emergence of structure at a system level arising from interactions between its constituent components [8]. Emergent behaviours are common in natural systems, such as the classic example of murmurations, the coordinated mass flights of starlings arising from simple interactions between a small number of neighbouring birds [9]. For satellite swarms, emergent behaviour has been proposed as a means for swarms to perform tasks ranging from collision avoidance [10] to high-resolution multi-point measurements [11]. Formal methods to verify and validate the emergent behaviour of intelligent satellite swarms have also been proposed [12].

In [13], the authors introduce the concept of satellite swarms, recount the technological developments that have enabled them, and state their key characteristics:

- Robustness
- Redundancy
- Large area coverage
- Lack of a hierarchical command structure
- Limited processing power per unit
- Self-organisation("swarm-intelligence")

The paper also explores the possible applications of satellite swarms, paying particular attention to a distributed radio telescope in Lunar orbit. As well as the potential appeal of satellite swarms, the paper recognises the inherent risks to space sustainability that satellite swarms can pose.

Swarm-based space architectures —which comprise multiple satellites or rovers operating collectively as a distributed system— have been proposed for astronomy [14], planetary exploration [15], and heliophysics [16] [6]. As well as these proposals, some key technology demonstration missions have already successfully flown and science swarms are under construction [16][17]. A selection of satellite swarm concepts is shown in Table 5.3.

3.2 Space Sustainability

The possibility of a runaway build-up of space debris —in which collisions create many small debris fragments which go on to create yet more collisions— was suggested as early as 1978 [18]. However, actions to avoid this 'Kessler Syndrome' have not proceeded in tandem with the build up of the space debris population. This problem was summarised by Gerald Brachet, formerly chairman of the United Nations' Committee on the Peaceful Uses of Outer Space (UN COPUOS), in 2016 [19].

> "*...our use of outer space since 1957 has been rather careless of its long-term sustainability. The situation might be compared to that of the 19th and 20th centuries with respect to maritime shipping and exploiting the oceans' resources where there was a wilful ignorance of the negative impact of pollution and a general blindness to the long-term effects of over-fishing*" [20]

The topic of space sustainability has become increasingly common in discussions of space policy as the dangers of space debris buildup have become more evident [19] [21]. In particular, accidental collisions and the intentional destruction of satellites have added huge amounts of space debris to Low Earth Orbit (LEO) [19] [22]. This is highlighted in Figure 3.1, which shows a snapshot of the observable debris population in Earth orbit with a particular focus on LEO. In 2017, roughly 18,500 observable Resident Space Objects (RSOs) were in orbit, with the large majority of these objects residing in LEO [23]. The figures from the European Space Agency (ESA) at the time of writing stand at 28,160 tracked objects and an estimated 128 million pieces of space debris larger than 1mm [24].

Mitigating the build up of space debris is necessary to preserve our access to space and space-enabled services, and is the goal of the Space Debris Mitigation Guidelines of the UN Committee on the Peaceful Uses of Outer Space [25] as well as various pieces of national legislation. Technical efforts to work towards space sustainability include the development of a satellite sustainability footprint [21] and determination and control of orbital carrying capacity [21] [26], as well as developing hardware such as servicing missions [27] [28], Active Debris Removal (ADR) missions [29] and de-orbiting kits [30].

A notable effort to improve sustainability is the Space Sustainability Rating developed by the World Economic Forum, the European Space Agency, Massachusetts Institute of Technology and the University of Texas at Austin. This rating —currently being operated by the Swiss Federal Institute of Technology Lausanne— is an aggregate rating taking into account factors including on-orbit fragmentation risk, collision avoidance capabilities, detectability, identification, trackability, data sharing, on-orbit servicing, collision avoidance, debris mitigation, and adoption of international standards [31]. While not incorporating all aspects of space sustainability, this rating was designed to encourage responsible behaviour in space by increasing the transparency of organisations' debris mitigation efforts.

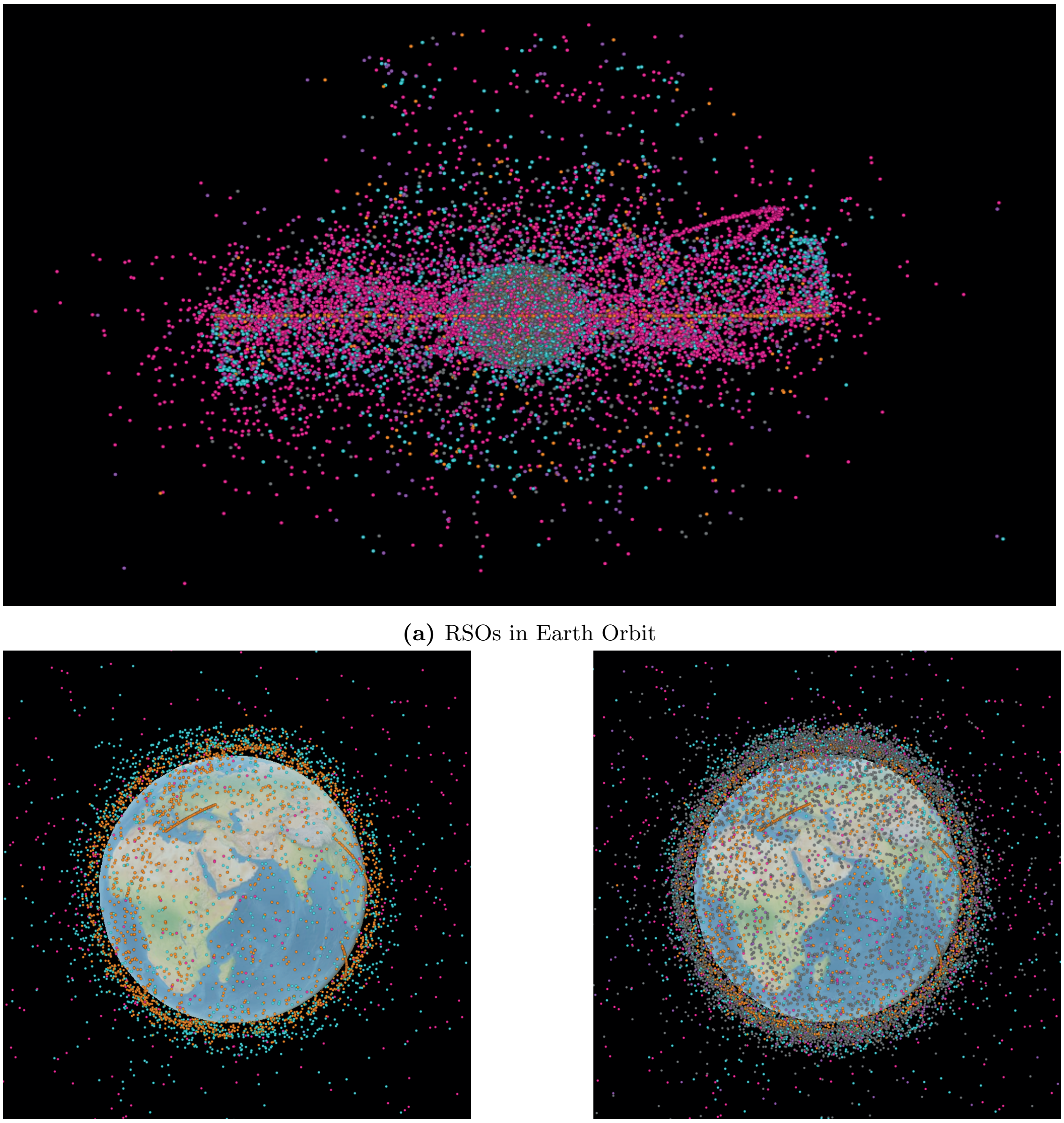

(a) RSOs in Earth Orbit

(b) RSOs in LEO not including debris

(c) RSOs in LEO including debris

Figure 3.1: Snapshots from the space domain awareness tool ASTRIAGraph [32] showing RSOs in Earth orbit. ASTRIAGraph is a framework that enables monitoring, assessment, and verification of space actor behaviour [33] and combines data from DigitalGlobe, JSC Vimpel, LeoLabs, Planet, SeeSat-L, the Union of Concerned Scientists, and USSPACECOM [32]. Figure 3.1a shows satellites and large items of space debris in all regions of Earth orbit, including the Geostationary Earth Orbit (GEO) ring and the GEO graveyard. Figure 3.1b and Figure 3.1c show LEO with and without large items of debris, respectively. Note that this figure shows large objects but does not show the clouds of smaller debris fragments that cannot be tracked from ground. The coloured dots represent different types of object: active satellites (orange), inactive satellites (cyan), rocket bodies (purple), uncategorised (magenta), and debris (grey).

3.3 Sustainable Swarms?

The increasingly likely prospect of operational satellite swarms raises the question of how to sustainably operate satellite swarms. The potential of satellite swarms to add to the debris population has been noted [13] [34], but swarm-specific space sustainability approaches have not yet been developed. As well as contributing many individual swarm agents to the growing population of space debris in orbit, mega-constellations or swarms comprising of numerous small satellites are difficult to track using current Earth-based sensor networks. Satellite swarms also increase the risk of collisions, particularly during end-of-life when small swarm agents cannot be manoeuvred to avoid collisions with functional satellite systems.

The distributed functionality which makes swarm missions so flexible also means that many individual swarm agents have to be disposed of at end-of-life, rendering traditional disposal methods problematic. Furthermore, the challenges of sustainably operating satellite swarms are as varied as the environments they could operate in — swarms used for planetary exploration will have to respect planetary protection policies while swarms engaged in Earth observation missions will have to be operated and safely de-orbited in an increasingly crowded LEO environment.

The potential applications of satellite swarms and the responsibility to assume a sustainable approach to space exploration are the basis of this thesis, which aims to answer an interesting question. How can we sustainably operate satellite swarms?

In this thesis we explore two routes to make satellite swarms more sustainable. The first is exploring whether inter-satellite links in a satellite swarm can be used to improve space situational awareness using the mega-constellation Starlink as an example. The second project is to explore the possibility of autonomous health monitoring within a satellite swarm as a means to predict and preempt satellite failures.

Chapter 4

Improving Space Situational Awareness with Swarm Localisation

4.1 Introduction

Improving the knowledge of the orbital state of satellites and debris is a crucial element of space sustainability, particularly Space Traffic Management (STM) and Space Situational Awareness (SSA). Already, as LEO becomes more crowded, satellite operators such as ESA are having to perform collision avoidance manoeuvres to dodge Starlink satellites — a precursor to the problems of widespread satellite swarms in orbit [35]. The distributed nature of satellite swarms contributes to the challenge of keeping track of satellites in orbit, but could also enable novel methods of improving SSA.

Within a satellite swarm, the interconnection of swarm agents allows cooperative localisation to be performed. This provides additional information to operators seeking to improve SSA, reduces dependency on ground stations, and provides a redundant method of localising swarm agents to any Guidance, Navigation, and Control (GNC) hardware on board the swarm satellites. The improved knowledge of orbital position can also benefit space sustainability beyond enabling SSA and STM. Knowing the precise location of satellites allows astronomers to time their observations to avoid satellite trails, which would otherwise saturate the sensitive detectors in large telescopes [36].

In this chapter, we explore to what extent collective localisation within a LEO swarm modelled on the Starlink constellation can improve SSA by establishing lower bounds on localisation performance. First, the Cramér-Rao Bound is introduced and explained via a toy problem. With this achieved, our simulation of Phase 1 of Starlink is explained and analysed, before the Cramér-Rao bound for each timestep of the satellite swarm simulation is calculated. The results are then discussed and placed in the context of other satellite localisation techniques before avenues for future work on this topic are discussed.

4.2 Cooperative Localisation

Cooperative localisation is a mature and well-studied field [37], [38], particularly due to work on *ad-hoc* wireless sensor networks for applications ranging from warehouse logistics to animal tracking [37], [38]. Despite the breadth and depth of research on cooperative localisation, this has yet to be widely applied to space systems engineering. In [39], the authors proposed a cooperative navigation system based on a satellite positioning constellation augmented by additional satellites at the Lagrange points. They found that their proposed system works well for the Earth-Moon system. More recently, cooperative localisation in small constellations with laser inter-satellite links has been studied in GEO and LEO [40]. However, as recently as 2020 research gaps have been identified in cooperative satellite navigation [41].

4.2.1 Formal Statement of the Cooperative Localisation Problem

The 2-dimensional cooperative sensor location estimation problem can be stated as follows [37]. Consider n nodes with unknown locations and m reference nodes (also known as anchor nodes) with exactly known locations. The problem is to estimate the $2n$ unknown coordinates $\theta = [\theta_x, \theta_y]$, where:

$$\theta_x = [x_1, x_2, ..., x_n] \text{ , } \theta_y = [y_1, y_2, ..., y_n]$$

given the location of the reference nodes, $[x_{n+1}, ..., x_m, y_{n+1}, ..., y_m]$ and a collection of pair-wise measurements $X_{i,j}$, where each $X_{i,j}$ is a measurement between nodes i and j. Assuming that not every node can connect to every other node, $H(i)$ defines the set of nodes with which node i can communicate. The node cannot communicate with itself, so $i \notin H(i)$ and $H(i) \subset 1, ..., n + m$.

4.2.2 Types of Measurement

When cooperatively localising nodes, the measurements between nodes can capture various properties, including the propagation time of the signals, the strength of received signals, or the angles from which signals are received. Three common methods are described below.

Received-Signal-Strength

Received-Signal-Strength (RSS) is simply a measurement of the strength of a signal at the receiver. If the initial signal strength is known, as well as the effects of propagation, then the distance to a source can be determined based on the strength of the received signal. However, RSS measurements are notoriously unpredictable [37].

Time-of-Arrival

Time-Of-Arrival (TOA) measurements are used to calculate distances between nodes by dividing the time of propagation of a signal by the velocity of propagation. For radio or optical signals propagating in a vacuum, this is simply $\frac{\Delta t}{c}$ where c is the speed of light and Δt is the time of flight.

This method requires the internal clocks of nodes and their biases to be known or estimated, or that the clocks are all synchronised. However, Rajan *et al.* showed in [42] that it is always possible to synchronise the clocks of a mobile anchorless network, subject to the constraint that each node has at least one 2-way connection to another node in the network. For our model swarm, this implies that the swarm can always be synchronised[1].

[1]As unconnected swarm agents are by definition not part of the swarm

Angle-of-Arrival

For Angle-Of-Arrival (AOA) measurements, the distance to neighbouring nodes is not measured but rather their direction. This provides complementary information to RSS and TOA measurements, but requires that the orientation of the nodes is either known or treated as an extra parameter to be estimated [37].

4.2.3 Cramér-Rao Bound

The Cramér–Rao Bound (CRB) provides a lower bound on the variance that can be achieved by any unbiased estimator [43] [44]. Essentially, the CRB is one of many performance bounds can be used to determine the 'best case' performance of an estimator at a given point with given information and using a given technique. Mathematically, the CRB for random measurements with the statistical model f($\mathbf{X}|\theta$) is given by:

$$\mathrm{Cov}(\hat{\theta}) \geq \left[\mathbf{E}\left[-\nabla_{\theta}\left(\nabla_{\theta} ln(\mathrm{f}(\mathbf{X}|\theta))^{T}\right)\right]\right]^{-1} \tag{4.1}$$

where $\mathrm{Cov}(\hat{\theta})$ is the covariance of the estimator, $E[\cdot]$ indicates the expected value, ∇_{θ} is the gradient operator with respect to the vector θ, the superscript ^{T} represents the transpose, and $ln(\mathrm{f}(\mathbf{X}|\theta)$ is the log-likelihood function [37]. The bound is affected by a number of parameters, including:

- The number of sensors with unknown locations (nodes) and the number of sensors with known locations (anchors)
- Sensor geometry
- Dimensionality (3D or 2D localisation)
- Type of measurement (*i.e.* RSS, TOA, or AOA)
- Link parameters
- Network topology (which pairs of sensors make measurements)

4.2.4 Calculating the Cramér-Rao Bound

The process to calculate the CRB is presented for the simple 2-dimensional case given as an example in *"Locating the nodes"* by Patwari *et al.* (2005) [37]. Following the methodology of Patwari *et al.*, the variance of the position of any given node i, σ_i is given by:

$$\sigma_i^2 \geq \left(\mathbf{F}^{-1}\right)_{i,i} + \left(\mathbf{F}^{-1}\right)_{i+n,i+n} \tag{4.2}$$

Where F is the $2n$ by $2n$ Fischer Information Matrix given by either:

$$F_A = \begin{bmatrix} \mathbf{F}_{yy} & -\mathbf{F}_{xy} \\ -\mathbf{F}_{xy}^{T} & \mathbf{F}_{xx} \end{bmatrix} \tag{4.3}$$

or,

$$F_{TR} = \begin{bmatrix} \mathbf{F}_{xx} & \mathbf{F}_{xy} \\ \mathbf{F}_{xy}^T & \mathbf{F}_{yy} \end{bmatrix} \tag{4.4}$$

The expression for the Fisher matrix depends on the type of measurement, with AOA using F_A and RSS and TOA using F_{TR}. The k, l elements of the submatrixes in Equation 4.3 and 4.4 are given by the equations:

$$[\mathbf{F}_{xx}]_{k,l} = \begin{cases} \gamma \sum_{i \in H(k)} (x_k - x_i)^2 / d_{k,i}^s & k = l \\ -\gamma I_{H(k)}(l)(x_k - x_l)^2 / d_{k,l}^s & k \neq l \end{cases} \tag{4.5}$$

$$[\mathbf{F}_{xy}]_{k,l} = \begin{cases} \gamma \sum_{i \in H(k)} (x_k - x_i)(y_k - y_i) / d_{k,i}^s & k = l \\ -\gamma I_{H(k)}(l)(x_k - x_l)(y_k - y_l) / d_{k,l}^s & k \neq l \end{cases} \tag{4.6}$$

$$[\mathbf{F}_{yy}]_{k,l} = \begin{cases} \gamma \sum_{i \in H(k)} (y_k - y_i)^2 / d_{k,i}^s & k = l \\ -\gamma I_{H(k)}(l)(y_k - y_l)^2 / d_{k,l}^s & k \neq l \end{cases} \tag{4.7}$$

Where d_{ij} is the true distance between the nodes i and j and $I_{H(k)}(l)$ includes information on the measurement topology. $I_{H(k)}(l) = 1$ if nodes k and l made a measurement with one another and $I_{H(k)}(l) = 0$ otherwise [2]. The other notation is the same as described in Section 4.2.1 and s is an exponent dependent on measurement type, with $s = 2$ for TOA and $s = 4$ for RSS and AOA. γ is a channel constant determined by the type of measurement, and is given by the following equations:

$$\gamma_{TOA} = \frac{1}{(v_p \sigma_T)^2} \tag{4.8}$$

where v_p is the propgation velocity of the signal and σ_T is the standard deviation of the time measurement used for TOA.

$$\gamma_{RSS} = \left(\frac{10 n_p}{\sigma_{dB} \log 10} \right)^2 \tag{4.9}$$

where n_p is the path-loss exponent that relates the rate at which power is lost over distance and σ_{dB} is the standard deviation of received power.

$$\gamma_{AOA} = \frac{1}{(\sigma_\alpha)^2} \tag{4.10}$$

where σ_α is the standard deviation of the angle measurements.

4.3 Toy Problem Exploring the Cramér-Rao Bound

To illustrate the sensitivity of the CRB to different network toplogies and link characteristics, we considered the setup shown in Figure 4.1 and recreated the results of [37].

[2] equivalently $I_{H(k)}(l) = 1$ if $l \in H(k)$

This numerical example is based on a 2D sensor network on a 20-m by 20-m area with K^2 sensors arranged on a regular grid of K rows and K columns. Four anchors are placed in the corners of the grid, leaving $K^2 - 4$ sensors with unknown positions. The lower bounds on localisation performance were calculated for three methods with the following characteristics:

- RSS with $\sigma_{dB}/n_p = 1.7$
- TOA with $\sigma_T = 6.1$ ns and $v_p = 3.8 \cdot 10^8$ ms^{-1}
- AOA with $\sigma_\alpha = 5°$

These values for earth-based wireless sensor networks are based on [37] and [45]. The results of the simulation are presented in Figure 4.1, which shows the Root Mean Square (RMS) value of the localisation bound using the relation:

$$CRLB_{RMS} = \left((1/n)\, tr\mathbf{F}^{-1}\right)^{1/2} \tag{4.11}$$

where $tr\mathbf{F}^{-1}$ is the trace of the inverse Fisher matrix. A sample calculation for the set-up shown in Figure 4.1 is given in Appendix B. The results show that AOA outperforms TOA and RSS whereas RSS and TOA exhibit comparable performance at high sensor densities. It is also important to note that increasing the number of sensors and increasing the sensor range both results in improved lower performance bounds [37].

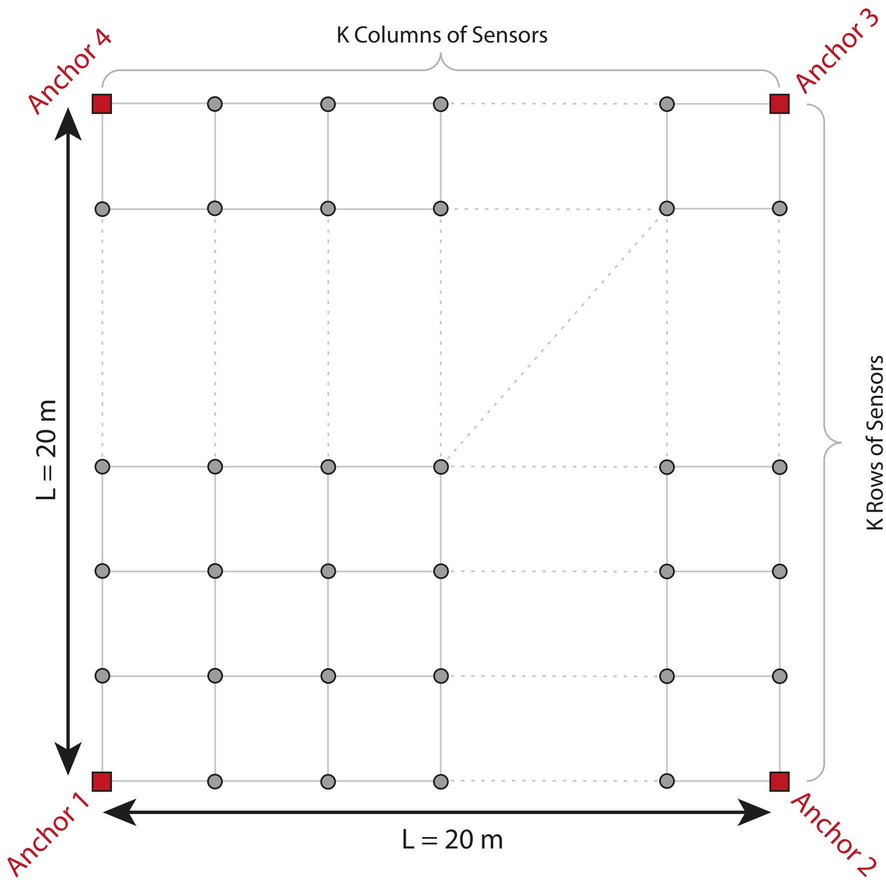

Figure 4.1: Set-up for a sensitivity analysis of the Cramér-Rao Bound in 2D recreating the results of *"Locating the nodes"* by Patwari *et al.* (2005) [37]. K^2 sensors are equally arranged on a grid with four reference sensors marked as red squares. The $K^2 - 4$ unknown locations sensors are marked with grey circles and are arranged on an L by L grid with $L = 20$m.

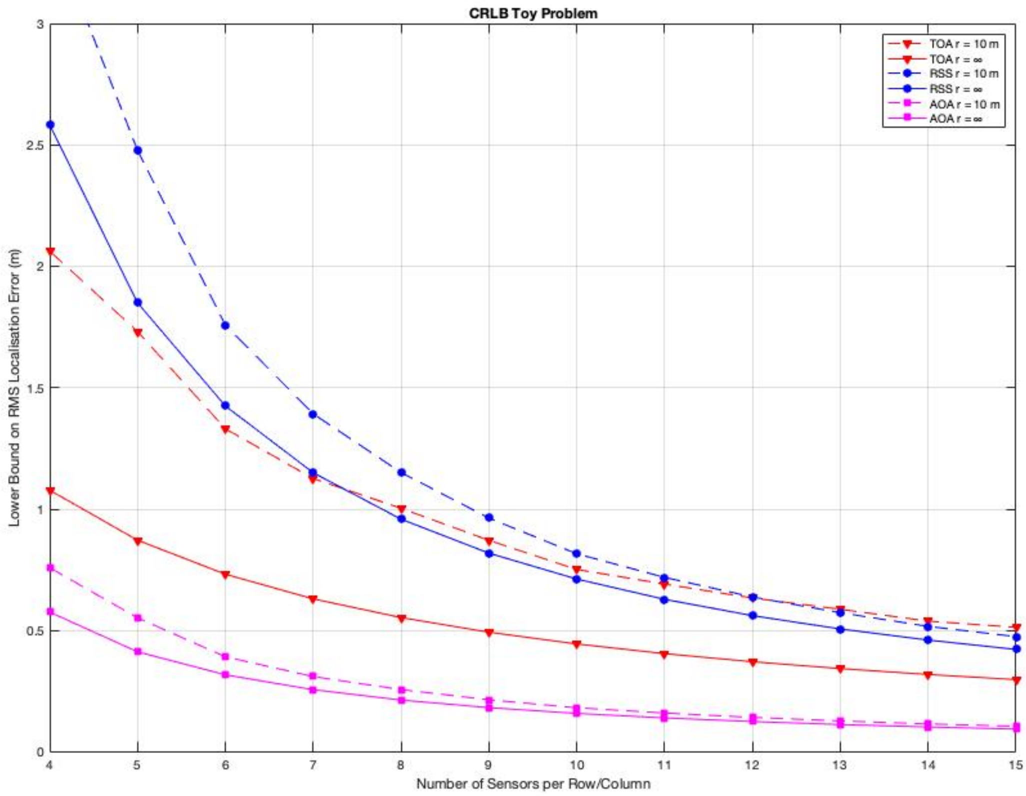

Figure 4.2: The Cramér-Rao Bounds for the network shown in Figure 4.1, comparing lower bounds of localization for RSS,TOA, and AOA methods. r denotes the radius over which sensors can make measurements, and for $r = \infty$ all pairs of sensors can make measurements with all other sensors.

4.4 Calculating the Instantaneous Cramér-Rao Bound for Starlink

To calculate the CRB for Starlink requires four steps. Firstly, the positions of the Starlink satellites have to be determined. From this, the network topology then has to calculated in the form of an adjacency matrix. Then, the position of the anchor nodes throughout the simulation must be calculated given the relative positions of the Starlink satellites and the ground stations on Earth. Finally, the satellite positions, adjacency, and anchor positions are used to calculate the CRB for each satellite at each timestep. The following sections introduce Starlink before proceeding through these four steps in order.

4.4.1 Introduction to Starlink

Starlink was chosen as a model swarm as it is a well-studied megaconstellation that meets our working description of a satellite swarm. Starlink is a LEO internet megaconstellation, in which thousands of satellites exchange data to provide low-latency internet [46]. These Inter-Satellite Links (ISLs) make Starlink a network of intercommunicating satellites collectively operating as a distributed system, and the internet communication enabled by Starlink is an emergent property of the system. Starlink is also an interesting model swarm as it has been noted as contributing to concerns about space sustainability [47] [48] and interference with ground-based astronomy [36] [49]. The ISLs between Starlink satellites and the resulting network topology have also been addressed in the literature [46] [50], as has the technical and economic performance of its internet network [51]. Starlink satellites have been deployed in batches of roughly 60 satellites at a time by the SpaceX Falcon 9 launcher continuously since 2019 with 1669 satellites in orbit at the time of writing. To achieve the high launch rates required to realise the full 32,000 satellite constellation, the satellites are flat-packed for launch as shown in Figure 4.3.

4.4.2 Simulating Starlink

To provide reference positions for simulations of cooperative localisation, a model Starlink was created using Python. The swarm consisted of 1584 satellites in Low Earth Orbit at an altitude of 550 km, corresponding to Phase 1 of the Starlink constellation. The parameters of this orbit are presented in Table 4.2. The swarm agents follow simple circular Keplerian orbits in an idealised 2-body system, ignoring perturbations such as aerodynamic drag or the J_2 effect. This dataset was published on IEEE DataPort™ as an open-access dataset [52], and the code was made available on GitHub [3].

The orbits were propagated using a built-in Polisastro function TWOBODY.PROPAGATION.VALLADO which propagates orbits using implementations of the algorithms in [53]. This method also outputs the position and velocity of each satellite in Cartesian coordinates.

Identifying Satellites

Following the methodology of Chaudhry & Yanikomeroglu [50] each Starlink satellite has a unique identifier with the format sXXYYY where XX is plane number and YYY is satellite number. For example, the first satellite in the first plane has the identifier s01001.

[3] https://github.com/CalumTurnerAstro/ConstellationEpheremides

Figure 4.3: Starlink satellites shortly before being deployed from a SpaceX Falcon 9. To achieve the high launch rates required to build the entire constellation, roughly 60 Starlink satellites are launched at a time. Image from WikiMedia.

Reference Frame

The reference frame for the positions and velocities of the simulated megaconstellation satellites is the Geocentric Celestial Reference System (GCRS) [54] with default parameters shown in Table Section 4.4.2. Satellite s01001 has initial position $[a, 0, 0]$ where a is the semi-major axis of the orbit.

Simulation Parameters

Simulation Parameters	
Parameter	**Value**
Number of Timesteps	573
ΔT	10 seconds
T	5730 seconds

Table 4.1: Timestep length (ΔT), total time (T), and number of time steps used to create the ephemerides for the Starlink mega-constellation. The total duration of the simulation is equal to one orbital period of a Starlink satellite.

The parameters used to run the simulation are shown in Section 4.4.2, where T is the total time of the simulation and ΔT is the duration of one timestep. The code used to create the Starlink ephemerides dataset can be readily modified to create ephemerides for other mega-constellations such as OneWeb or Kuiper, and is publicly available under a permissive MIT license at **this link**. This code does have some limitations, however:

- Despite sharing the same constellation design, the ephemerides of the simulated satellites do not necessarily reflect the actual orbital positions of Starlink satellites.
- The simulated megaconstellation consists of a single shell of satellites with the same altitude, whereas proposed megaconstellations will eventually consist of several shells
- Orbital perturbations such as the J_2 effect or aerodynamic drag are not taken into account.

The ephemerides data has the format shown in Appendix A. The data was exported from a Pandas DataFrame with multi-level indexing, and the first two columns of the .csv file are indexes for each individual satellite and each individual timestamp.

Model Swarm Orbital Parameters		
Parameter	**Value**	**Notes**
Altitude	550 km	LEO
Number of Planes	72	Updated from [50]
Satellites per Plane	22	Updated from [50]
Inclination i	53°	
Orbital Period T	1.59 hours	
Total Satellites	1584	

Table 4.2: Orbital parameters of the model swarm, based on the innermost shell of Phase I of Starlink [55]. The orbital planes were assumed to be evenly spaced, as were the satellites within each plane. Note that the numbers are different from those presented in [50], as they have been updated to reflect the most recent plans for Starlink based on the information in an Federal Communications Commission (FCC) filing dated April 17, 2020.

Simulation Reference Frame	
Parameter	**Value**
Observation Time	J2000.000
Position of the observer relative to the barycenter	[0, 0, 0] m,
Velocity of the observer relative to the barycenter	[0, 0, 0] m,

Table 4.3: Parameters of the reference frame used to create the ephemerides for the Starlink megaconstellation.

4.4.3 The Starlink Network

Starlink will eventually be connected with optical inter-satellite links allowing the system to transmit information and carry internet traffic, but publicly available information about this system is sparse. To determine which links were possible within the inter-satellite network, we considered three constraints: visibility, range, and hardware limitations. Each constraint is described in detail below, and the line-of-sight constraint is illustrated in Figure 4.4

- **Visibility:** Also referred to as Line-Of-Sight (LOS), swarm agents can establish links with one another only if they are visible to one another. Figure 4.4a demonstrates how occlusion by a central body affects this situation in LEO, the orbital regime of our Starlink example. In LEO, the presence of a central body imposes a maximum link length of 5016 km km assuming that the ionosphere is completely opaque up to an altitude of 80 km, as shown in Figure 4.4b.
- **Hardware:** Range and LOS place physical constraints on potential links, but the design of the swarm satellites themselves also affect which links are possible. In Starlink, for example, the number of laser links that each satellite can support is limited in practice by the number of optical heads on each satellite.
- **Range:** The distance between swarm agents determines whether or not they can establish a link.

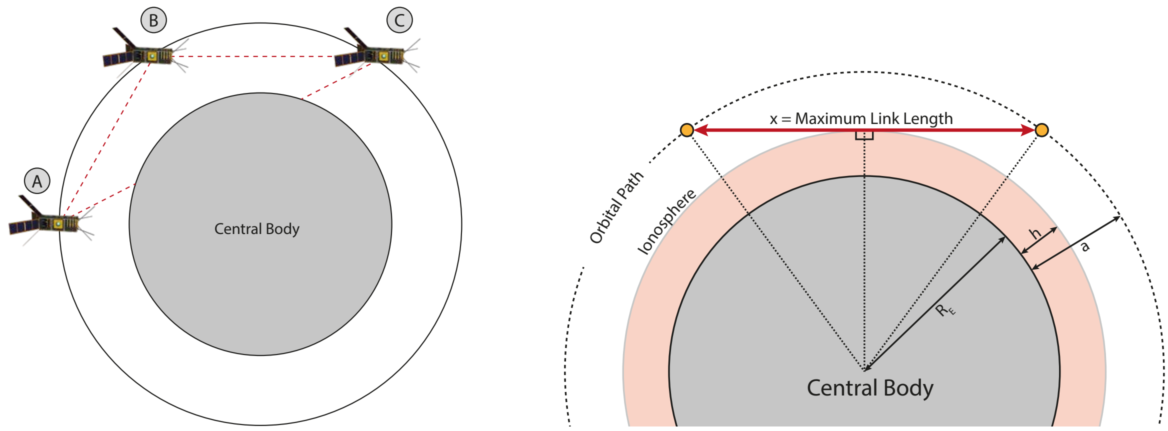

(a) Link Visibility **(b)** Geometrical Set-up

Figure 4.4: Geometrical constraints due to a central body for a satellite swarm in LEO. Figure 4.4a shows how Line Of Sight (LOS) is affected by the presence of a central body. Swarm agents A and C can both create links with the intermediate agent B, but not with each other. Figure 4.4b shows the geometrical set-up for calculating the how the radius of the Earth (R_E) and the height of the ionosphere (h) place an upper limit on the range of a LOS link in LEO at an altitude a. Simple geometry gives a maximum link length of $x = 2\sqrt{(R_E + a)^2 - (R_E + h)^2} = 5016$ km [46] [50] [41].

The topology of the Starlink network —the shape of the inter-satellite network— is determined by which satellites are connected, as constrained by the physical constraints of visibility and distance and the technological constraints of the satellites themselves. This choice can be optimised by innovative network design, taking into account the time taken to establish links as well as the challenge of acquiring and tracking links between satellites on crossing orbital planes. In [50], the authors classify and analyse the time-varying links available in the Starlink constellation[4]. A similar analysis using the most up-to-date orbital configuration of the Starlink mega-constellation is shown in Figure 4.5 and 4.6. As the results show, the greatest number of possible connections occurs at mid-latitudes of roughly 60°.

The orbital dynamics of LEO constellations means that the number of inter-satellite links a single satellite can make varies over the course of an orbit. This a fundamental consequence of LEO orbits, in which satellites travel at roughly 27,000 miles per hour [46].

To calculate the CRB for Starlink, we assume a Plus Grid (+Grid) topology, in which satellites are connected to 4 nearby satellites — two in the same orbital plane and two in neighbouring planes as described in [46]. This is shown in Figure 4.7a for the full Starlink network. Figure 4.7b shows the +Grid topology for a single satellite, and this network topology is used throughout the rest of this chapter.

[4]Though the orbital parameters the authors used for Starlink are now out of date.

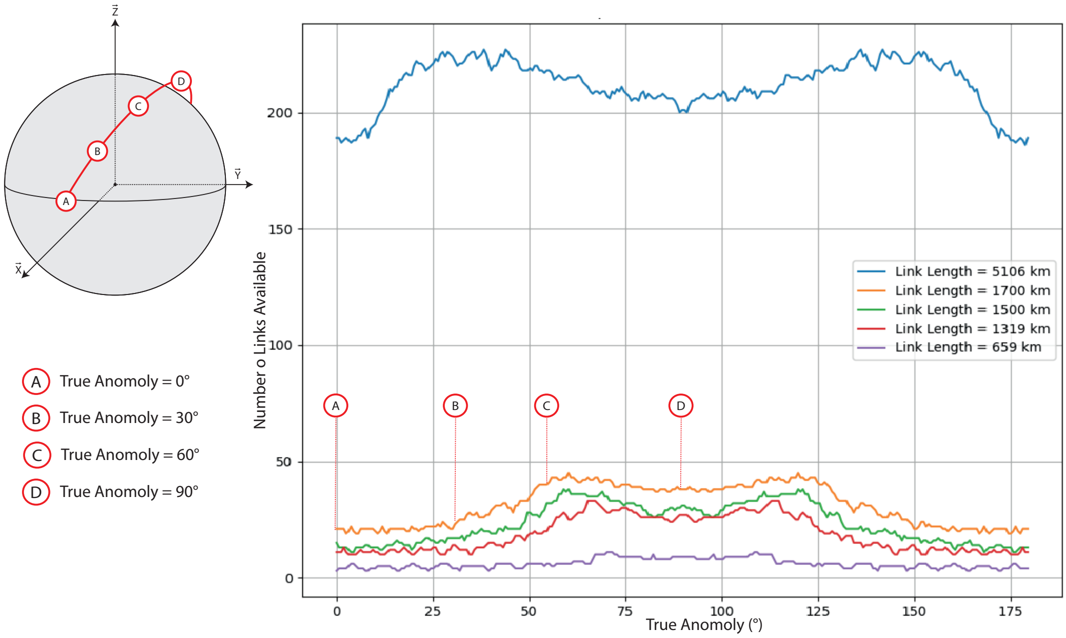

Figure 4.5: Graph of the number of possible links against true anomaly for swarm agent *s01001* with a variety of maximum link lengths from 659 km to 5016 km. The snapshots A-D are rendered in Figure 4.6. The orbital dynamics of Starlink mean that the number of possible connections is highly time-varying. As the graph shows, the greatest number of possible connections occurs at mid-latitudes of roughly 60°, and unsurprisingly a greater maximum link length results in a greater number of possible connections.

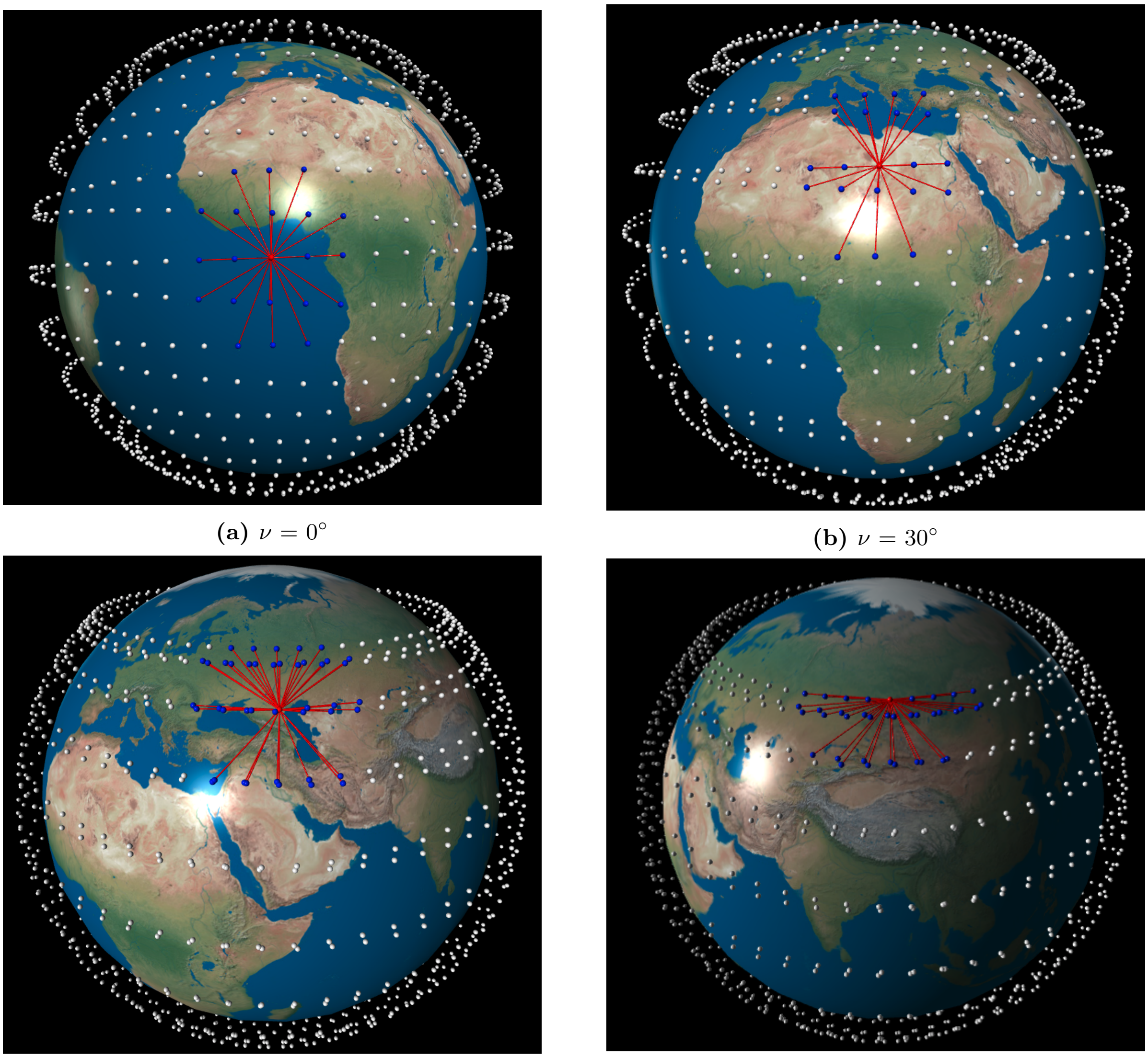

(a) $\nu = 0°$ **(b)** $\nu = 30°$ **(c)** $\nu = 60°$ **(d)** $\nu = 90°$

Figure 4.6: Possible connections in the Starlink network highlighted at different points in the orbit for a maximum link length of 1700 km. A graph of the time-varying number of links at each point is shown in Figure 4.5. The snapshots are identified by the true anomaly of the satellite shown red, swarm agent *s01001*. Connected satellites are shown in blue. The figure demonstrates the same result as Figure 4.5, namely that the number of possible links in Starlink Phase 1 is greatest at latitudes of roughly 60° and least above the equator.

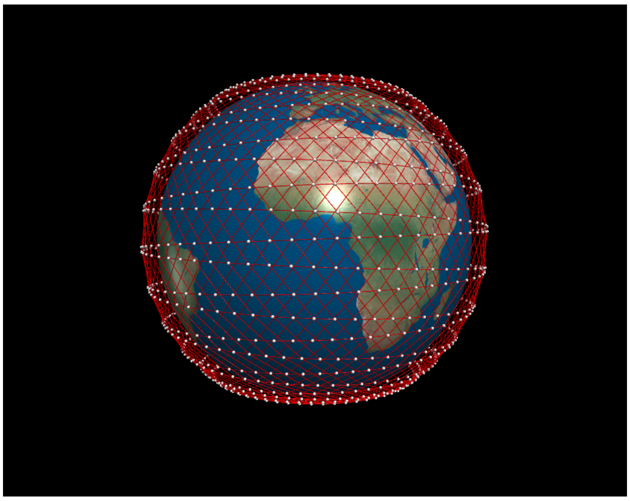

(a) Full Starlink Network

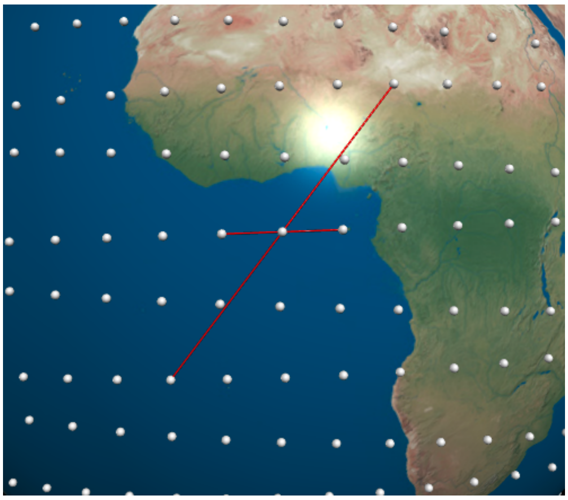

(b) Connections for one satellite

Figure 4.7: Full network of the Starlink mega-constellation assuming a +grid topology as described in [46]. Figure 4.7a shows the full network, which is made from repeated patterns of the form shown in 4.7b. This network assumes that each satellite in limited to four connections due to hardware constraints.

4.4.4 Location of Anchors

To calculate the CRB for Starlink requires the location of anchor nodes to be determined. We first explored how the number and distribution of ground stations would affect the number of connected satellites, assuming that the anchor nodes for the network would communicate with n_a ground stations spaced evenly over the Earth's surface [5]. To determine which satellites would act as anchor nodes, we calculated the visibility of satellites from ground stations using the equations detailed in [56]. The geometric set-up is shown in Figure 4.8, and the derivation of the distance between a ground station and a satellite starts with the cosine law for triangles:

$$r^2 = R_E^2 + d^s - 2 \cdot R_E \cdot d \cdot \cos(\frac{\pi}{2} + \epsilon_0) \tag{4.12}$$

Rearranging this equation by using the quadratic equation and some simplification gives the following equation:

$$\frac{2 \cdot R_E \cdot \cos(90 + \epsilon_0) \pm \sqrt{4 \cdot R_E^2 \cdot \cos^2(\frac{\pi}{2} + \epsilon_0) - 4 \cdot (R_E^2 + r^2)}}{2} \tag{4.13}$$

Applying simple trigonometric identities ($\cos^2\theta - \sin^2\theta = 1$, $\cos\theta = \sin(\frac{\pi}{2} - \theta)$, and $\sin(-\theta) = \sin\theta$), then it is possible to obtain the following equation after some trivial rearranging:

$$d = R_E \left[\sqrt{\left(\frac{r}{R_E}\right)^2 - \cos^2\epsilon_0} - \sin\epsilon_0 \right] \tag{4.14}$$

Finally substituting $r = R_E + a$ gives the maximum distance to a satellite at an elevation angle of ϵ_0 above the ground station's horizon:

$$d = R_E \left[\sqrt{\left(\frac{a + R_E}{R_E}\right)^2 - \cos^2\epsilon_0} - \sin\epsilon_0 \right] \tag{4.15}$$

To find the maximum possible distance at which a satellite would be able to be tracked by a ground station, we set $\epsilon_0 = 0$, giving $\cos^2\epsilon_0 = 1$ and $\sin\epsilon_0 = 0$. The equation simplifies to:

$$d = R_E \left[\sqrt{\left(\frac{a + R_E}{R_E}\right)^2 - 1} \right] \tag{4.16}$$

Plugging in the values of a=550km and $R_E = 6371$ km gives a maximum distance of 2704 km, in line with the results presented in [56]. Calculating the satellites which are connected to the ground stations gives the positions of the anchor nodes for the Starlink network. Section 4.4.4 shows the positions of anchor nodes for different numbers of anchors, under the assumption that the n_a ground stations are evenly distributed over the surface of the Earth. As the figure shows, many Starlink satellites can connect to a single ground station under the assumption that $\epsilon_0 = 0$, that is that satellites are visible on the horizon. However, in practice,

[5] Neglecting for now geographically realistic locations for ground stations.

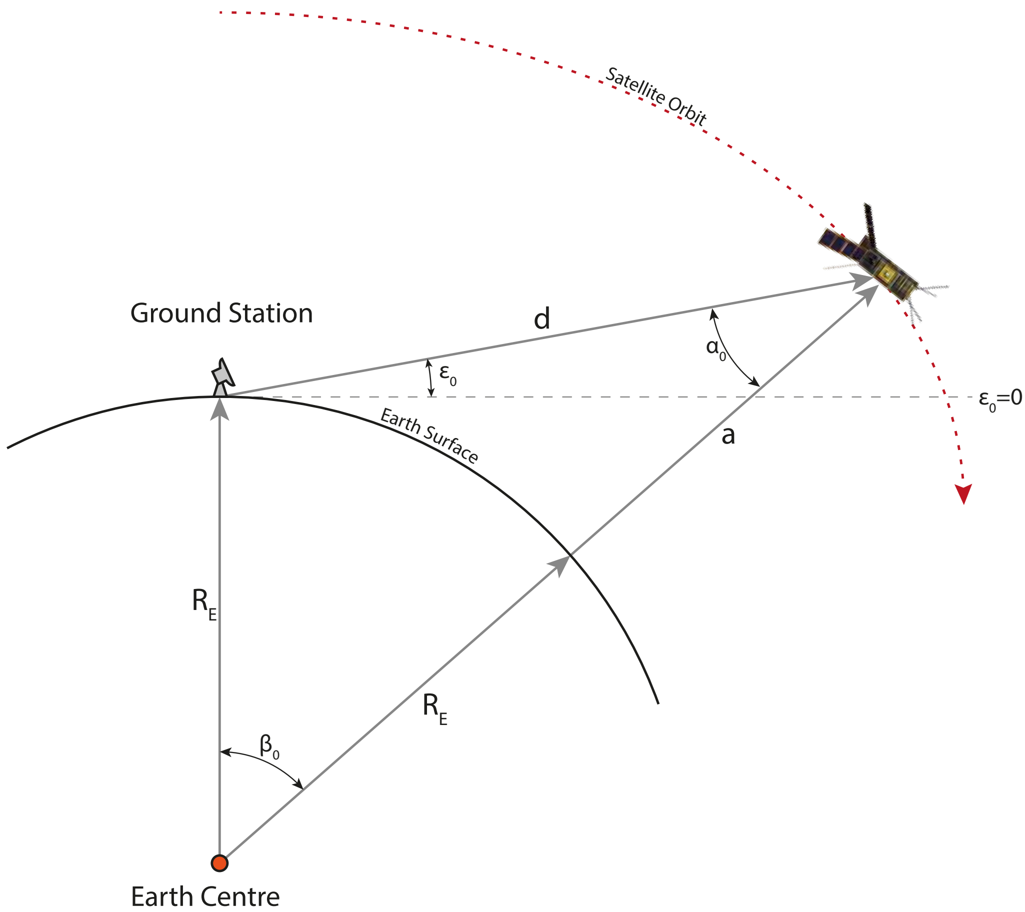

Figure 4.8: A diagram of the geometric set-up used to calculate the visibility of satellites from a ground station. The satellite has an altitude of a and makes an angle of ϵ_0 with the ground station's local horizon. The maximum distance at which the satellite is visible can be found by determining d. Diagram adapted from [56].

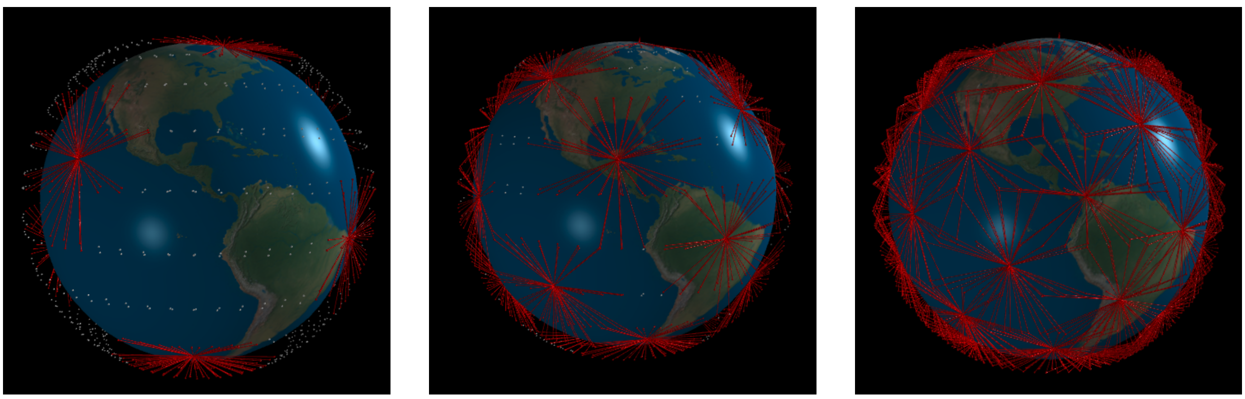

(a) $n_a = 10$ **(b)** $n_a = 25$ **(c)** $n_a = 50$

Figure 4.9: Visualisation of the anchored nodes for the Starlink network for an increasing number of randomly distributed ground stations n_a. The satellite positions are shown in white and the red lines connect ground stations to the anchored nodes with an assumed value of $\epsilon_0 = 0°$.

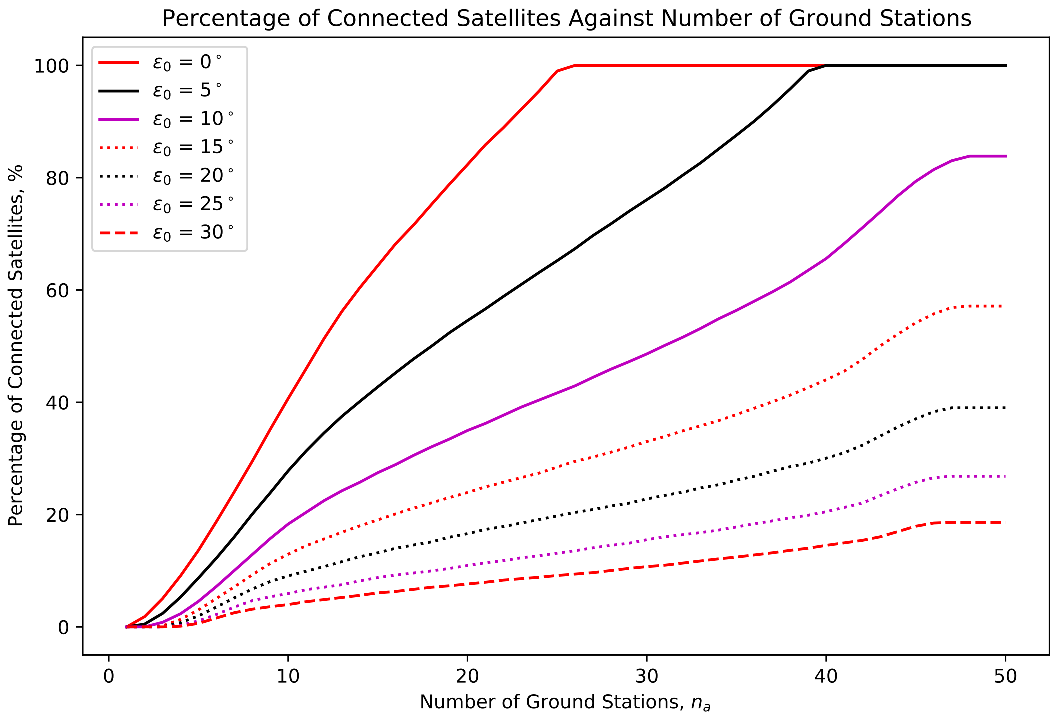

Figure 4.10: The graph shows the number of connected satellites against the number of equally distributed ground stations, n_a. Note that for small enough values of ϵ_0 and large enough numbers of ground stations the percentage of connected satellites maxes out — that is, every satellite is connected to a ground station. Increasing the value of ϵ_0 drastically reduces the total number of satellites connected. A safe margin for ϵ_0 avoids barriers such as hills, forests, or buildings [56]. This value ranges from ϵ_0 =0° to 30° [57], [58], and the visibility range d for each value of ϵ_0 is as follows: 0°=2704 km, 5°=2205 km, 10°=1815 km, 15°=1518 km, 20°=1294 km, 25°=1123 km, and 30°=993 km.

barriers such as hills, forests, or buildings mean that satellite operators often define a safe margin for ϵ_0 that avoids these barriers [56]. This value ranges from $\epsilon_0 = 0°$ to 30° [57], [58]. Plugging these values into Equation (4.15) gives the results plotted in Figure 4.10. The value of ϵ_0 and the number of ground stations n_a determine what percentage of the constellation is connected to a ground station, as shown in Figure 4.10. An increasing number of ground stations and a decreasing value of ϵ_0 both —in line with intuition— increase the percentage of connected satellites.

In reality, however, Starlink ground stations are not evenly distributed over the Earth, instead being constrained by geography, politics, accessibility, and cost. Figure 4.11 shows the location of 87 planned or active Starlink ground stations as based on regulatory filings in the USA, Chile, UK, France, Australia, and New Zealand. The names and locations of all ground stations are provided in Appendix C. Providing these locations to the Starlink simulation shows that an average of 126^{+9}_{-12} satellites are connected over the course of an orbit, *i.e.* between 7.8% and 9.1% of the total number of satellites[6]. Bearing in mind the trends shown in Figure 4.10, the relatively low proportion of connected satellites despite $n_a = 87$ ground stations can be attributed to the relatively conservative value of $\epsilon_0 = 40°$ [59]. There are 341^{+18}_{-22} satellite-to-ground-station connections in total, *i.e.* many satellites are connected to multiple ground stations. This arises as the coverages of some ground stations overlap, as shown in Figure 4.11.

[6]Note that these percentages will increase as more ground stations are added to the Starlink network

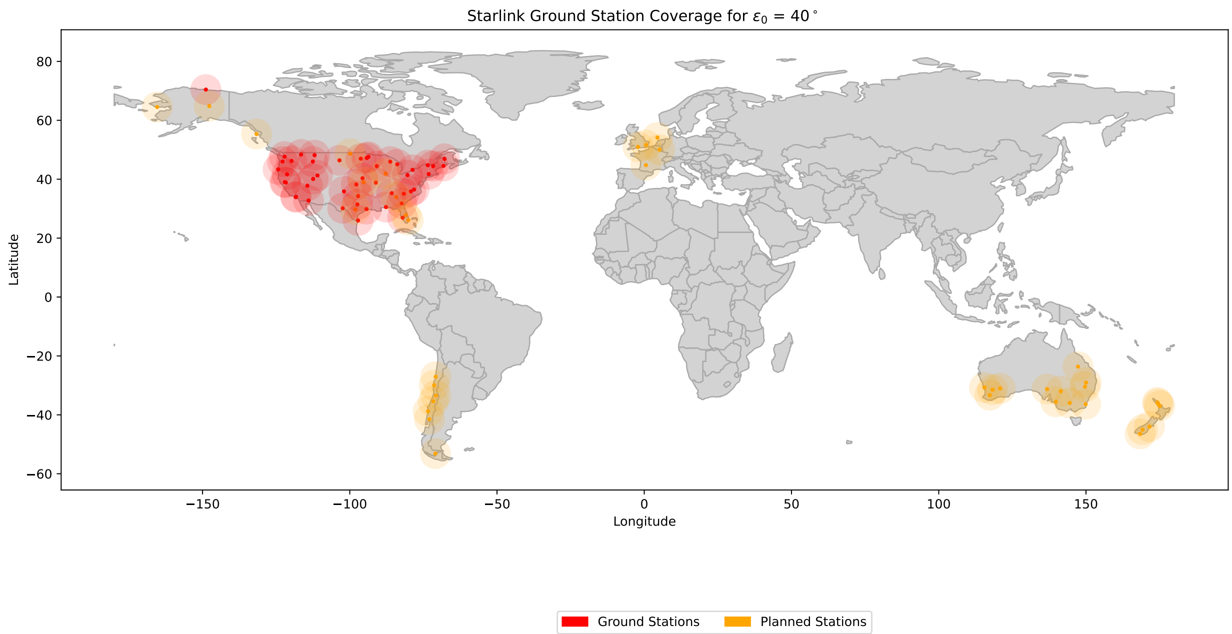

Figure 4.11: The locations of 87 planned and active Starlink ground station and their coverage assuming ϵ_0 = 40° [59]. The locations of the ground stations are substantiated by filings with the Federal Communications Commission in the USA, República De Chile Ministerio De Transportes Y Telecomunicaciones Subsecretaría De Telecomunicaciones in Chile, Autorité de Régulation des Communications Électroniques et des Postes in France, the Office of Communications in the UK, the Australian Communications and Media Authority and the Ministry of Business, Innovation & Employment, Radio Spectrum Management in New Zealand. All latitudes and longitudes are approximate (correct at the town/city level). Setting $\epsilon_0 = 40°$ gives a visibility range of $d = 812$ km. As Starlink is a US company, the active ground stations are predominantly located in the USA. The names and locations of all ground stations are provided in Appendix C.

4.4.5 Calculating the Cramér-Rao Bound for Starlink

With the positions, network, and anchor locations defined for Starlink Phase 1, it is now possible to calculate the CRB for the mega-constellation. The mathematical framework is an extension of that used in Section 4.2.4 but as opposed to one large Fisher matrix for the entire constellation, we calculated an individual Fisher matrix for each Starlink satellite at each timestep. This choice reduced the run-time of the simulation by reducing the size of the matrix inversion required to calculate the CRB, which is computationally intensive. The choice to calculate individual Fisher matrices is also more appropriate for the distributed systems such as satellite swarms. Assuming TOA measurements, the formulae used to calculate the CRB for a single Starlink satellite with position $[x, y, z]$ are:

$$\mathbf{F} = \gamma \begin{bmatrix} \mathbf{F}_{xx} & \mathbf{F}_{xy} & \mathbf{F}_{xz} \\ \mathbf{F}_{xy}^T & \mathbf{F}_{yy} & \mathbf{F}_{yz} \\ \mathbf{F}_{xz}^T & \mathbf{F}_{yz}^T & \mathbf{F}_{zz} \end{bmatrix} \tag{4.17}$$

where:

$$\mathbf{F}_{xx} = \sum_{i \in H(k)} (x - x_i)^2 / d_i^s \tag{4.18}$$

$$\mathbf{F}_{yy} = \sum_{i \in H(k)} (y - y_i)^2 / d_i^s \tag{4.19}$$

$$\mathbf{F}_{zz} = \sum_{i \in H(k)} (z - z_i)^2 / d_i^s \tag{4.20}$$

$$\mathbf{F}_{xy} = \sum_{i \in H(k)} (x - x_i)(y - y_i) / d_i^s \tag{4.21}$$

$$\mathbf{F}_{xz} = \sum_{i \in H(k)} (x - x_i)(z - z_i) / d_i^s \tag{4.22}$$

$$\mathbf{F}_{yz} = \sum_{i \in H(k)} (y - y_i)(z - z_i) / d_i^s \tag{4.23}$$

Where d_i is the distance between the Starlink satellite and connected node i with position $[x_i, y_i, z_i]$, and $H(k)$ consists of the four connected satellites in the +Grid network as well as any ground stations within range. Inverting the Fisher matrix $\mathbf{F}$ gives the CRB matrix whose diagonals are the best achievable x,y, and z location variances. To generate a single figure of merit, the Root Mean Square Error (RMSE) value of the localisation bound was calculated using the relation:

$$\text{CRLB}_{RMSE} = \left((1/n)\, tr\mathbf{F}^{-1}\right)^{1/2} \tag{4.24}$$

4.4.6 Results

Calculating the instantaneous CRB for all Starlink satellites required the Fisher matrix to be calculated and inverted for 1584 satellites at each of 573 time steps — a total of 907,632 matrices to be calculated. To obtain a single figure of merit, equation 4.24 was used to determine the CRB RMSE. Calculating the CRB for Starlink during a full orbital period of $T = 5730$ seconds gives the results shown in Figure 4.12. The average RMSE is shown as a dashed black line, and has a fairly constant value of roughly 10.15 m. The value of the CRB varies between a maximum of 36.5 m and a minimum of around 2 m. Figure 4.12 also shows the CRB for a single satellite (*s01001*) over the course of its orbit. The value is mostly close to the average, but has two prominent peaks at $t = 1430$ and $t = 4300$ seconds. There is also a noticeable dip in the value at $t = 4750$. These three situations (labelled A,B, and C) are rendered in Section 4.4.6.

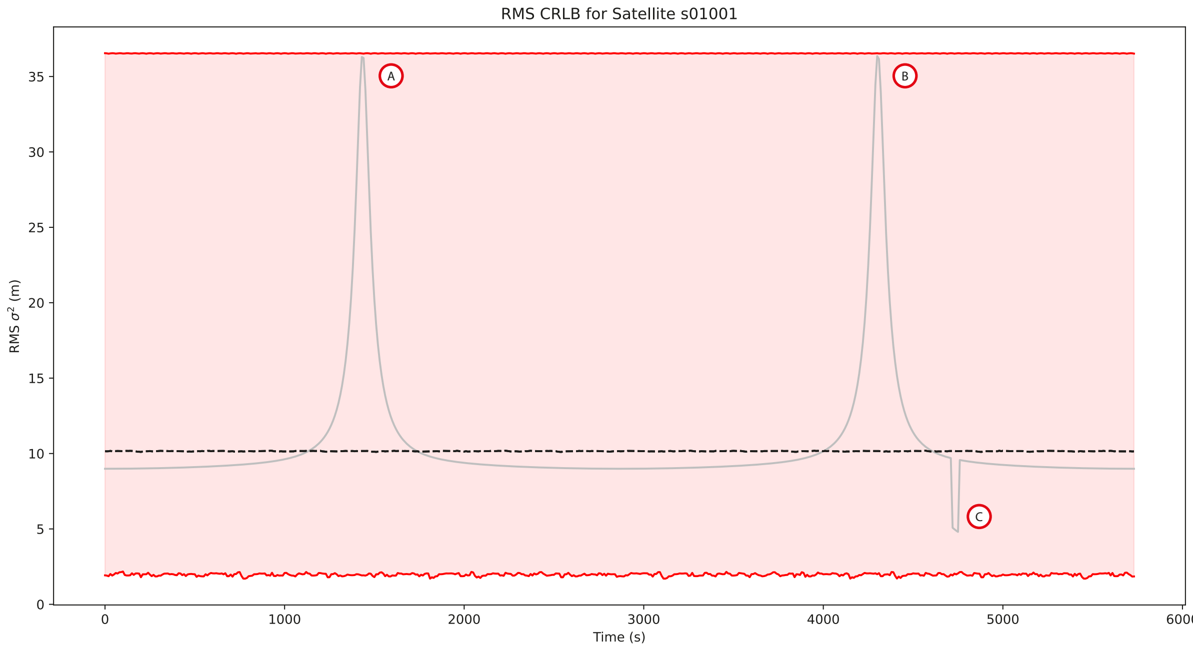

Figure 4.12: The average CRB for Starlink constellation is shown as a dashed black line, and indicates that the Starlink satellites can be localised to within 10.15 metres on average. The shaded red area indicates the area between the maximum (36.5 m) and minimum (2m) CRB. The CRB for satellite *s01001* is shown in grey, and has prominent peaks (labelled A and B) and a trough labelled C. Taking *s01001* as a reference, the results indicate that it is possible to localise satellites to within less than 10 metres for the majority of its orbit. The position of *s01001* is rendered in Section 4.4.6.

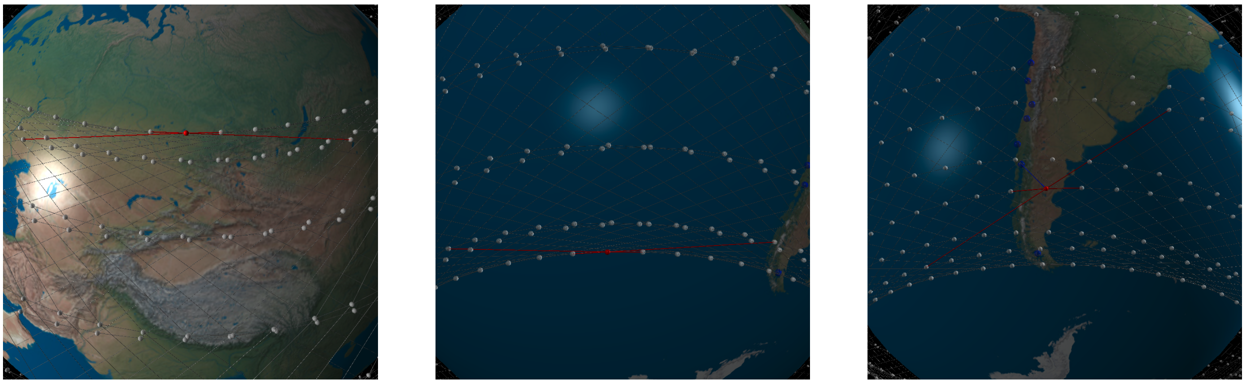

(a) Situation A, t=1430 s **(b)** Situation B, t=4300 s **(c)** Situation C, t=4750 s

Figure 4.13: Snapshots of the satellite *s01001* in the Starlink simulation at the times highlighted in 4.12. For situation A, at a time of t=1430 s, satellite *s01001* is at the highest latitude in its orbit. Situation B, at a time of t=4300 s, the satellite is at its lowest latitude. Situation C shows satellite *s01001* passing over Tierra del Fuego at the southernmost tip of Chile. In each situation, the connections between satellite *s01001* and other nodes (including ground stations) are shown in red (blue). These three situations correspond to extremes in the CRB for satellite *s01001*.

Inspecting Section 4.4.6 and Figure 4.12, as well as the ground tracks shown in Figure 4.14 and Figure 4.15 allows us to interpret the peaks and troughs in the CRB for satellite *s01001*. Situations A and B occur when the satellite is at the highest and lowest latitude in its orbit. The two renderings in Section 4.4.6 show why this occurs — the geometrical arrangement of connections with other satellites is less evenly distributed than for the rest of the orbit. This results in an effect similar to dilution of precision in Global Positioning Satellites, where aligned satellites results in a lower position accuracy. Figure 4.14 reveals the reason for the lower CRB in situation C — as satellite *s01001* passes over a ground station in southern Chile, the connection to the ground station provides more information, reducing the value of the CRB.

The pass of *s01001* above a ground station is shown in greater detail in Figure 4.15, which shows the ground track over Tierra del Fuego and a detailed plot of the CRB for *s01001*. The CRB drops by around 50% as soon as it is within communication range of the ground station at Puerto Montt. While the CRB is reduced by the connection to a ground station, the underlying trend in the CRB is unchanged. This trend is driven by the changing geometry of the Starlink network, and can be seen as the gradual decrease in the plot of *s01001*'s CRB even while the satellite is in range of the Puerto Montt ground station.

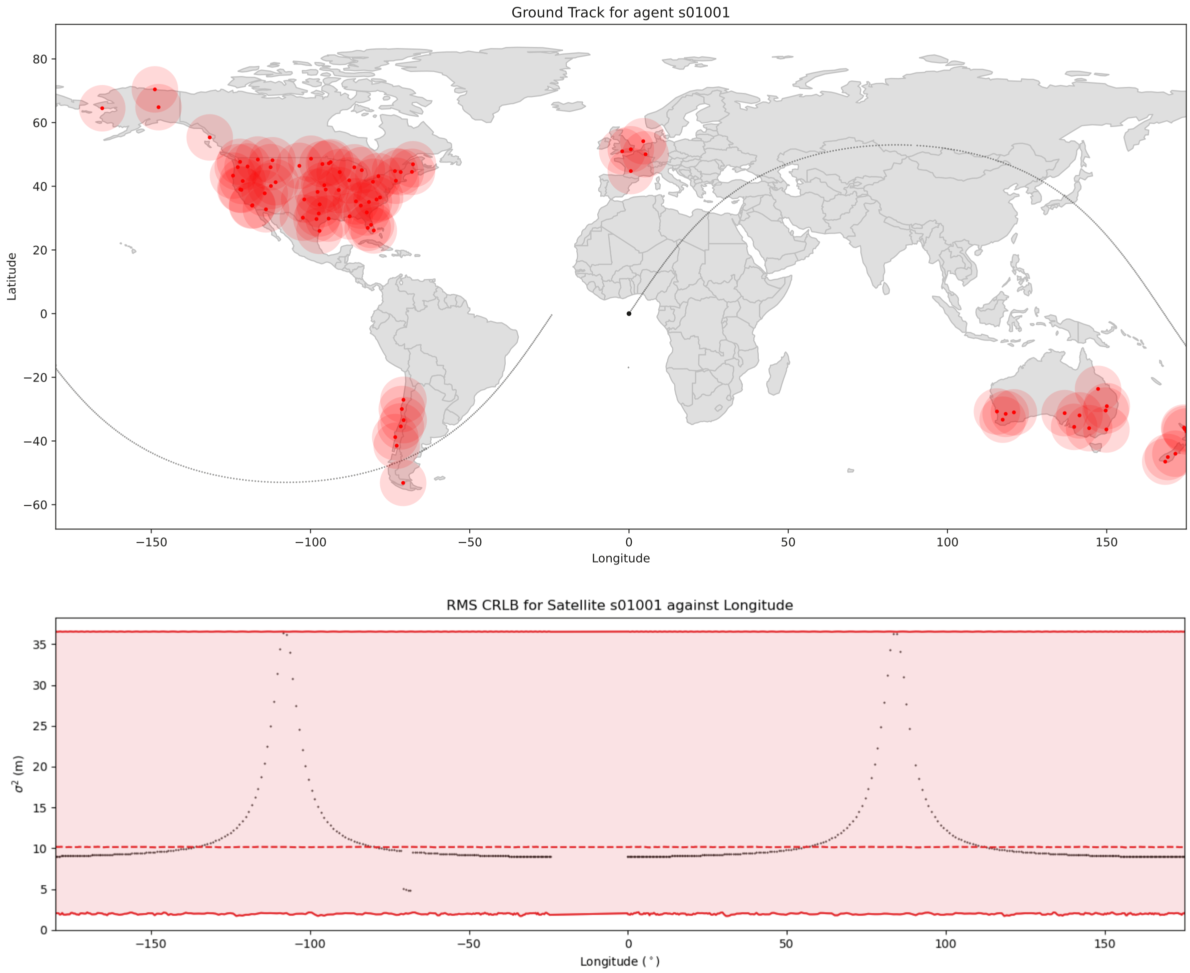

Figure 4.14: The upper figure shows the ground track for satellite *s01001* as well as the position of the Starlink ground stations. The lower figure shows the CRB against longitude, with the average CRB for he constellation shown as a dashed red line and the area between the maximum and minimum values for the constellation are shaded in red. Referring to the two plots, it is clear that the peaks in the CRB correspond to the highest and lowest latitudes for *s01001*'s orbit, and that the trough in the CRB occurs when *s01001* is in range of a ground station in South America. The pass of *s01001* over the ground station is shown in detail in Figure 4.15.

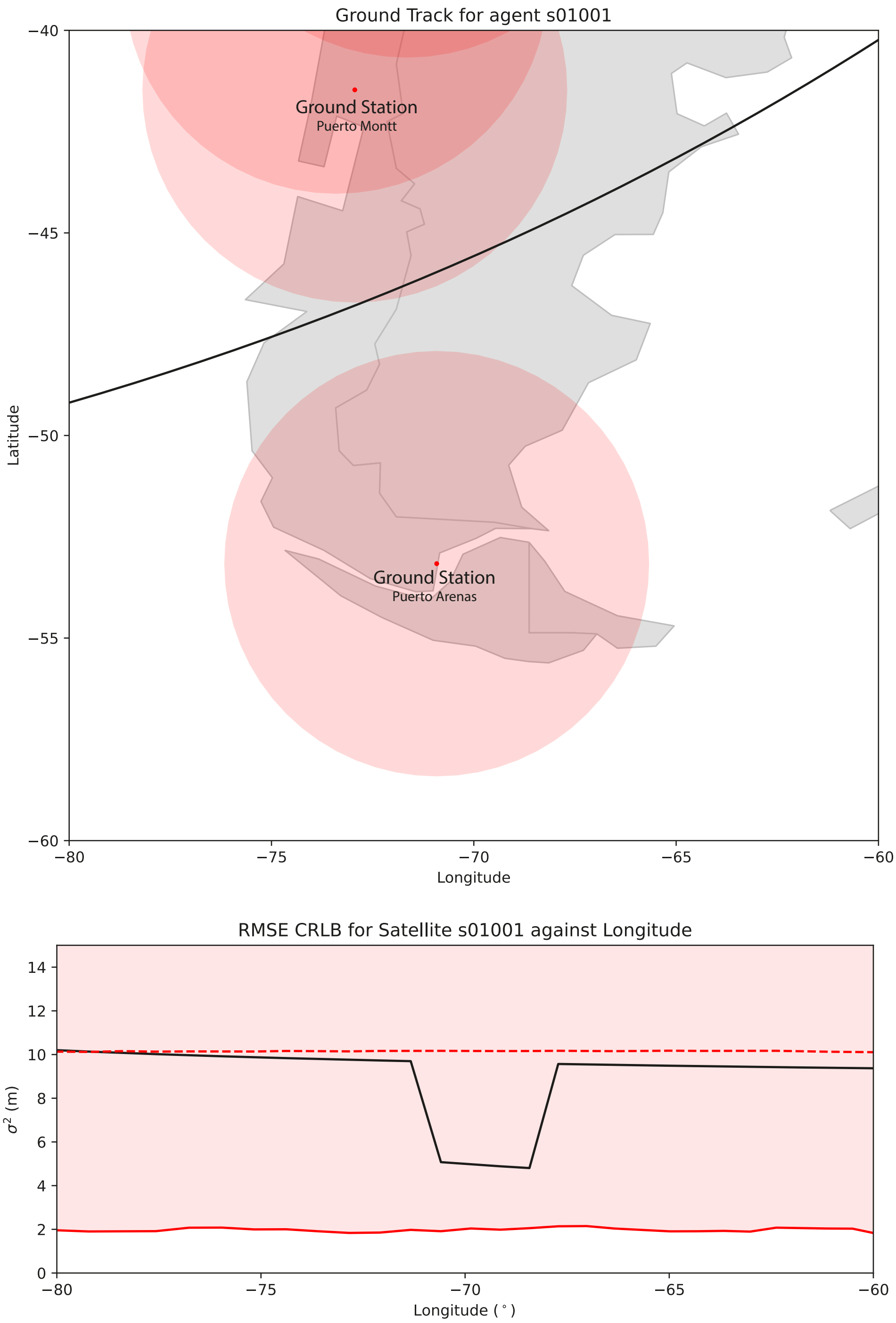

Figure 4.15: The figure shows satellite *s01001* passing over Tierra del Fuego at the southernmost tip of Chile, as well as the CRB during this pass. Comparison of the two plots shows that the CRB drops by roughly 50% while it is in range of the ground station at Puerto Montt. The overall trend in the CRB, which is a gradual decrease driven by the geometry of the Starlink network, continues even while *s01011* is in range of the ground station.

4.4.7 Discussion

The results indicate that the position of Starlink satellites can be determined from inter-satellite measurements to an average RMSE of approximately 10.15 metres for the majority of their orbit. However, this result is highly dependant on the value of γ used to calculate the CRB and also ignores the dynamics of the system, as explained in the following two sections.

Assumptions on γ

The calculations presented in Section 4.4.5 show that the value of the CRB is highly sensitive to the value of γ, with larger values of γ resulting in smaller CRB values. This implies that the accuracy achievable with cooperative localisation in Starlink is dependent on the characteristics of the inter-satellite links. Unfortunately, the details of these inter-satellite links are not publicly available, but it is possible to make some initial statements of the link characteristics required for cooperative localisation in Starlink. The value of γ for TOA measurements is:

$$\gamma = \frac{1}{(v_p \sigma_T)^2} \tag{4.25}$$

where the expression for σ_T given in [37] is:

$$\sigma_T \geq \frac{1}{8\pi^2 B T_s F_c^2 \mathrm{SNR}} \tag{4.26}$$

where B is the bandwidth in hertz, F_c is the centre frequency in hertz, T_s is the duration of the signal, and SNR is the signal-to-noise ratio, ignoring the effects of multi-path communications[7]. The value for γ used in the simulation of Starlink was $\gamma = 29,8605$. From Equation (4.25) and assuming that the velocity of propagation v_p is $3{\cdot}10^5\ \mathrm{km \cdot s^{-1}}$, this means that link characteristics which satisfy:

$$\frac{1}{B T_s F_c^2 \mathrm{SNR}} \leq 4.81 \cdot 10^{-7} \mathrm{s} \tag{4.27}$$

could provide at best the performances presented in Section 4.4.6. Repeating the analysis for a range of link characteristics based on existing satellite hardware could allow a technical trade-off to be performed. Other aspects of the inter-satellite links, such as equipment duty cycles, could also affect inter-satellite links — for example, in [41], the author considered the duty cycle of communications in satellite pairs and small satellite constellations.

System Dynamics

The results presented in the previous section present the RMSE on location estimation without considering system dynamics. In other words, a predictive filter that considers the state dynamics such as an Extended Kalman Filter could provide better performance than predicted by the CRB. Intuitively, modelling the system dynamics provides more information than just inter-satellite measurements, thus meaning that a more accurate localisation is achievable.

[7] Which is a reasonable assumption to make for satellites in orbit

Comparison to Existing Localisation Methods

This performance is comparable to the performance of Global Navigation Satellite System (GNSS) and recent research into localisation using laser inter-satellite links for small constellations in Low Earth Orbit [40], both of which achieve performances of roughly 2 meters in LEO. Our results are somewhat higher, but given that they do not yet incorporate state dynamics it should be possible improve upon these results with more sophisticated modelling. Possible methods to improve the simulation are described in the following section.

4.5 Future Work

While this result is a promising first step, there are several improvements to be made to this simulation in future work. For example, our methodology could be applied to other planned or growing mega-constellations, such as Kuiper or OneWeb [60]. Simulating these mega-constellations would increase the breadth of our work and could indicate if this approach could be a feasible way of increasing space situational awareness in mega-constellations in general.

The simulation of Starlink developed in this chapter was sufficient for the purposes of determining the CRB, but there is room for improvement in the the modelling of the mega-constellation. For example, including the J_2 effect would provide a more accurate set of ephemerides. The satellites in Phase 1 of Starlink orbit at a fairly low altitude of 550 km, and as such would also be affected by subtle aerodynamic drag. Both these perturbations can be calculated using `Poliastro`, and their inclusion in future simulations will improve the accuracy of our results.

Changing the network topology of Starlink could also provide interesting results. In [46], the authors discuss the topology of the inter-satellite network in LEO satellite mega-constellations, showing that a repetitive network of latitude-dependent patterns provides an efficient network compared to traditional +Grid designs from the point of view of internet traffic. Adopting a latitude-dependent network topology could possibly reduce the high CRB values experienced at high and low latitudes for Starlink satellites.

The results presented here assume that ground stations can be used as anchor nodes, but another approach would be to only perform relative navigation between the Starlink satellites themselves. This decouples the problem of satellite localisation into relative positions within the swarm and the absolute position of the swarm itself

With the improvements above implemented and the revised lower performance bounds of localisation in Starlink determined, an intuitive next step will be to actually employ a cooperative localisation technique to determine the positions of Starlink satellites. Our proposed approach is first to perform a centralised calculation — one where all the information is assumed known and the locations of all the Starlink satellite are calculated at once. Following this centralised localisation method, we will apply 'off-the-shelf' distributed localisation methods to simulate each Starlink satellite determining its position independently, which is more in keeping with the swarm focus of this research.

Once the improvements mentioned above have been implemented, this study will comprise a novel body of work and hopefully the basis for further research. The ephemerides described in 4.4.2 have already been published on IEEE DataPort™ as an open-access dataset to aid other researchers, and we plan to perform more analyses and publish further research into anchor-free localisation in Starlink by the end of the year. The impacts of autonomous distributed satellite systems such as Starlink on the orbital environment is not yet clear, and research which helps understand or mitigate these impacts is vital to ensure our exploration of space remains sustainable.

Chapter 5

Satellite Health Estimation

In this chapter, a method that could enable the autonomous health estimation of swarm agents is presented based on studies of CubeSat subsystems and Markov modelling of satellite subsystems. This builds on previous work from a summer project at TU Delft, which is described in detail in Section 5.1. The parameters for a single satellite health figure of merit are presented in section Section 5.2, and ongoing work using Markov chains to weight the parameters is shown in section Section 5.3.1. Other ongoing work comparing the swarm satellite health parameter to real CubeSat failures is presented in Section 5.3.2, and finally next steps and potential future applications of this approach are discussed in Section 5.4.

5.1 Satellite Health Indicator

In *"End-of-Life for Satellite Swarms"* by Turner and Rajan (2020) [4], which was presented at the 71^{st} IAC, we proposed a satellite health indicator which would allow us to convert from satellite telemetry to a single figure of merit for satellite health. This indicator differentiates between factors which are absolutely critical for continued mission operations, and those which simply degrade the performance of a swarm satellite[1]. Out approach follows the use of composite indicators in other fields; in [31] the authors note that:

> " *Composite indicators have been increasingly recognised as powerful instruments for bench-marking, performance monitoring, policy analysis and public communication in the fields of society, environment and economy.*" [31]

Specifically, composite indicators have been suggested to quantitatively represent concepts ranging from sustainable energy development [61] to human development [62], and mathematical frameworks have been developed to create these composite indicators [63]. Our satellite health indicator is our first approximation of a single figure-of-merit for satellite health, and takes the form:

$$\theta = \prod_{i=1}^{n} \alpha_i^c P_i^c \cdot \sum_{j=1}^{m} \alpha_j P_j \tag{5.1}$$

The value of the satellite health indicator is denoted by θ, and is expressed as a product of n critical factors $P_i^c \dots P_n^c$ with normalised weightings α_i^c. The sum includes m non-critical factors $P_j \dots P_m$, with normalised

[1] Note that the notation has been updated since Turner and Rajan (2020) [4]

weights α_j Each factor is scaled to the range $0 \leq P_i^c, P_j \leq 1$, using 1 to denote perfect functionality and 0 to denote a complete failure of the relevant subsystem [64]. As such, the satellite health indicator maps telemetry to the aggregate health of a satellite's subsystems represented as a single real number in the range $0 \leq \theta \leq 1$.

In our proposed satellite health indicator, critical factors are included as a product and noncritical factors as a sum. Any failure in a critical factor is reflected in a total satellite health indicator of 0, whereas failure of a noncritical system simply degrades the health of the satellite. The first step towards a viable satellite health indicator is to identify these factors and their weightings.

5.2 Choosing Parameters for the Satellite Health Indicator

We approached the problem by identifying the subsystems present in generic swarm satellites. Based on the assumption that swarm agents are likely to be relatively small and inexpensive [13], [65], we assumed that the subsystems of CubeSats would be a good model for swarm satellite subsystems. Both CubeSats and swarm satellites are likely to be less reliable and use a greater proportion of Commercial Off-The-Shelf (COTS) parts than traditional monolithic satellite systems. Table 5.1 shows typical CubeSat subsystems and their purpose.

Cubesat Subsystems	
Subsystem	**Purpose**
Structure	Structural support
On-board Data Handling	Controlling data uplink and downlink
Telemetry, Telecommand, and Control	Command and communication with Earth
Electrical Power System	Producing, conditioning, and distributing power
On-board Software	On-board computation and operations
Attitude Determination and Control System	Determining and control satellite attitude
Propulsion	Changing satellite orbit
Thermal Control System	Monitoring and controlling satellite temperature

Table 5.1: Typical CubeSat systems and their purpose [66].

We chose to represent each parameter in Table 5.1 as a parameter in the satellite health indicator, with the exception of the thermal control system. The thermal control system was assumed to be passive and therefore likely to outlive the other subsystems, following the reasoning presented in [65]. Bearing in mind our working definition of satellite swarms as *a network of intercommunicating satellites exhibiting complex emergent behaviour, collectively operating as a distributed system*, we require an extra parameter — an inter-satellite link. The chosen parameters are presented in Table 5.2, alongside the notation used to referred to them and whether they are critical or non-critical factors. Three parameters — Telemetry, Tracking, and Command (TTC), GNC, and the payload were identified as non-critical. Again following the reasoning of [65], satellites without payloads or active GNC subsystems can still be useful to a satellite swarm by acting as relay stations. Similarly, swarm satellite which cannot be reach from ground via the TTC subsystem can still cooperate with other swarm satellites through their Inter-Satellite Link (ISL).

Table 5.3 shows a selection of satellite swarms, their missions and current status, as well as a checklist of which of the satellite health parameters are present in their designs. The table demonstrates that the satellite health parameters are broadly applicable to a range of satellite swarms. Figure 5.1 shows a labelled

Satellite Health Indicator Parameters			
Subsystem	**Critical**	**Symbol**	**Weighting**
ISL	✓	P_{isl}	α_{isl}
TTC	✗	P_{ttc}	α_{ttc}
Software & On-Board Data Handling (OBDH)	✓	P_{obdh}	α_{obdh}
Attitude Determination and Control System (ADCS)	✓	P_{adcs}	α_{adcs}
GNC	✗	P_{gnc}	α_{gnc}
Electrical Power System	✓	P_{eps}	α_{eps}
Payload	✗	P_{pl}	α_{pl}
Structure & Mechanical	✓	P_{mech}	α_{mech}

Table 5.2: Chosen parameters of the satellite health indicator based on subsystems that could be present in any given swarm agent. The satellite health indicator parameters were chosen to be sufficiently generic that they can be applied to any given swarm agent regardless of the mission design.

diagram of a generic CubeSat and the physical subsystems represented by the satellite health parameters.

	Swarm Mission Concepts				
	← More Mature			Less Mature →	
Name	STARLING-1	HELIOSWARM	OLFAR	ANTS	APIS
Destination	Low Earth Orbit	Earth Orbit	Earth Orbit	Lunar Orbit	Earth Orbit
Purpose	Tech Demo	Heliophysics	Radio Astronomy	Exploration	Heliophysics
Status	Launching 2021	Under construction	Studied Concept	Concept	Concept
Reference	[17]	[16]	[14]	[15]	[7][6]
P_{isl}	✓	✓	✓	✓	✓
P_{ttc}	✓	✓	✓	✗	✓
P_{obdh}	✓	✓	✓	✓	✓
P_{adcs}	✓	✓	✓	✓	✓
P_{gnc}	✓	✓	✓	✓	✓
P_{eps}	✓	✓	✓	✓	✓
P_{pl}	✗	✓	✓	✓	✓
P_{mech}	✓	✓	✓	✓	✓

Table 5.3: A collection of swarm mission concepts at varying degrees of maturity showing the diverse potential applications of swarm missions and the applicability of the satellite health indicator parameters. The table shows that the chosen satellite health parameters are common to a variety of swarms.

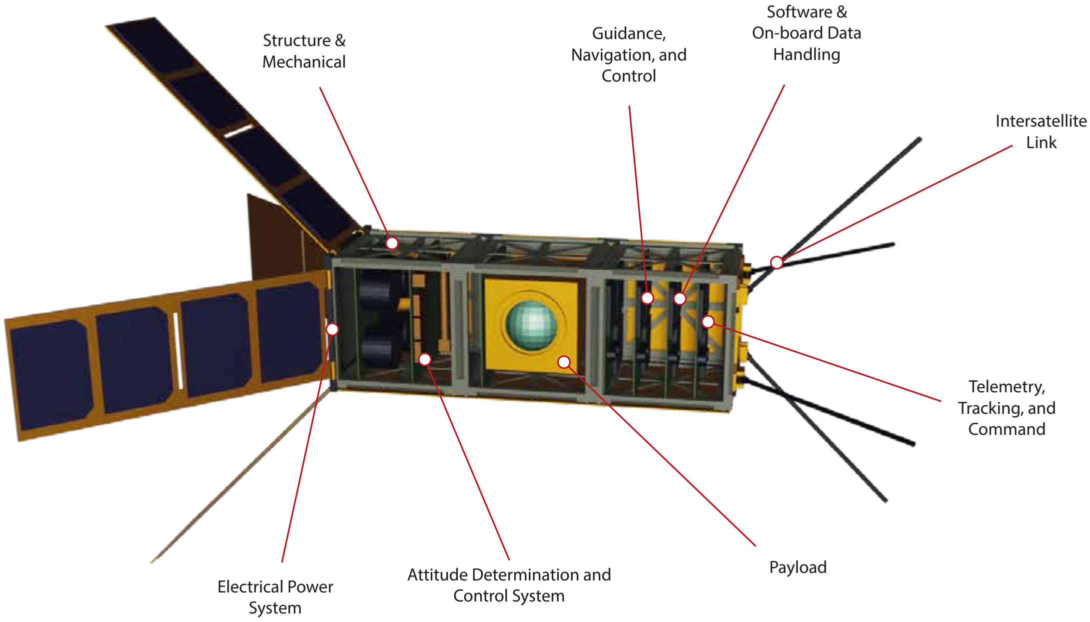

Figure 5.1: A cutaway diagram of a CubeSat showing the principle subsystems, each of which is the physical basis for one of the satellite health indicator parameters shown in Table 5.2. Note that this is not an engineering drawing, but a rather a generic model of a CubeSat.

5.3 Ongoing Work

Our research on satellite health estimation is still ongoing, and at the time of writing we are pursuing two different lines of investigation into developing the satellite health indicator. The first investigation is to use a Markov model of generic swarm satellites to determine which subsystems most often lead to satellite failures, using this information to weight the parameters in the satellite health indicator. The second investigation is to examine failures in CubeSats to determine how often we can expect swarm satellites to fail. These two projects are presented in section 5.3.1 and 5.3.2, respectively

5.3.1 Weighting the Satellite Health Parameters

With the satellite health parameters defined, our ongoing task is to determine the weightings of each parameter. These reflect the relative importance of each factor to the satellite's overall health. Following the methodology reported in [65], we have created a Markov model of a generic swarm satellite. The Markov model is shown in Figure 5.2, and shows 19 different states in which the swarm satellite could be, ranging from complete functionality to system failure, with 17 intermediate states representing degraded functionality. Any failure of the electrical power supply, on-board data handling, or structure of the CubeSat (including deployable antennas and solar panels) is treated as an immediate system failure. The probability of transition from state to state are based on reported subsystem failure rates [65] [67] [68]. We are in the process of optimising the Markov model and comparing it to observed failure rates in CubeSats, which are presented in the following section.

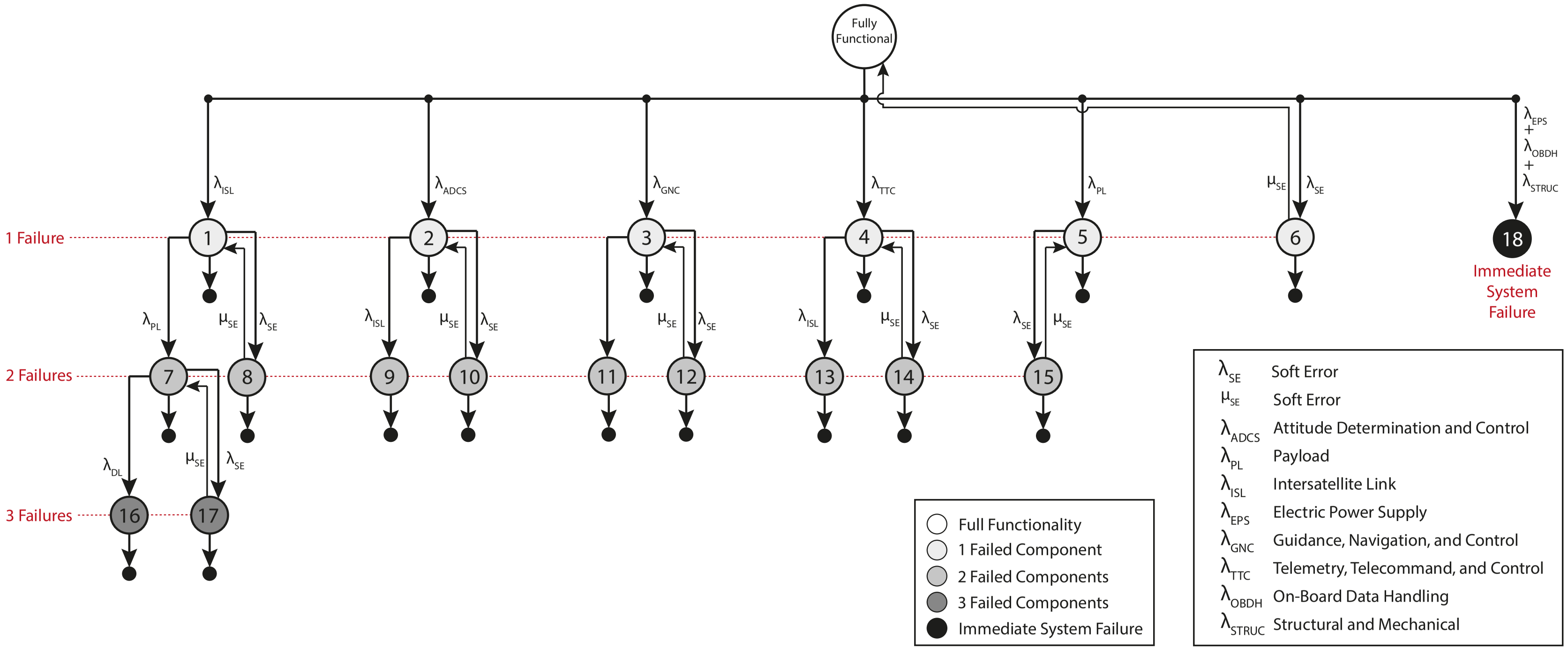

Figure 5.2: Adapted Markov Chain for a swarm satellite taking into account the satellite health parameters, adapted from the work presented in [65]. Progressively darker states represent increasing number of subsystem failures, and state number 18 (immediate system failure) is present at the end of each branch but reduced in size for clarity.

5.3.2 Exploring CubeSat Satellite Failures

Initial efforts to estimate the reliability of CubeSats were stymied by small sample sizes [68] and the nascent technology involved [65], but more than 1500 CubeSats have now been launched, allowing for statistical analysis of CubeSat failures [69]. In this section we explore the launch rates of CubeSats since 2002 to infer how reliable swarm satellites might be, again assuming that CubeSats provide a good model for swarm satellites. The data in this section is available at CGEE CubeSat database [2] and was kindly provided by scientists at the Brazilian Observatório de Tecnologias Espaciais. The database lists 1515 satellites launched between December 2nd 2002 and April 29th 2021.

Figure 5.3 shows the cumulative numbers of CubeSats launched since 2002 sorted by sector — military, civil, university, or commercial. The number of launches per year is also shown. The graph shows that while most CubeSat launches were initially educational satellites from universities, the total number of CubeSats in orbit is now dominated by commercial satellites. The data also shows a downturn in launch rates coincident with the COVID-19 pandemic in 2019 and 2020. Other studies of CubeSat failures suggest that the reliability of a CubeSat is dependent on the class of CubeSat, with university projects more likely to experience mission failure [70].

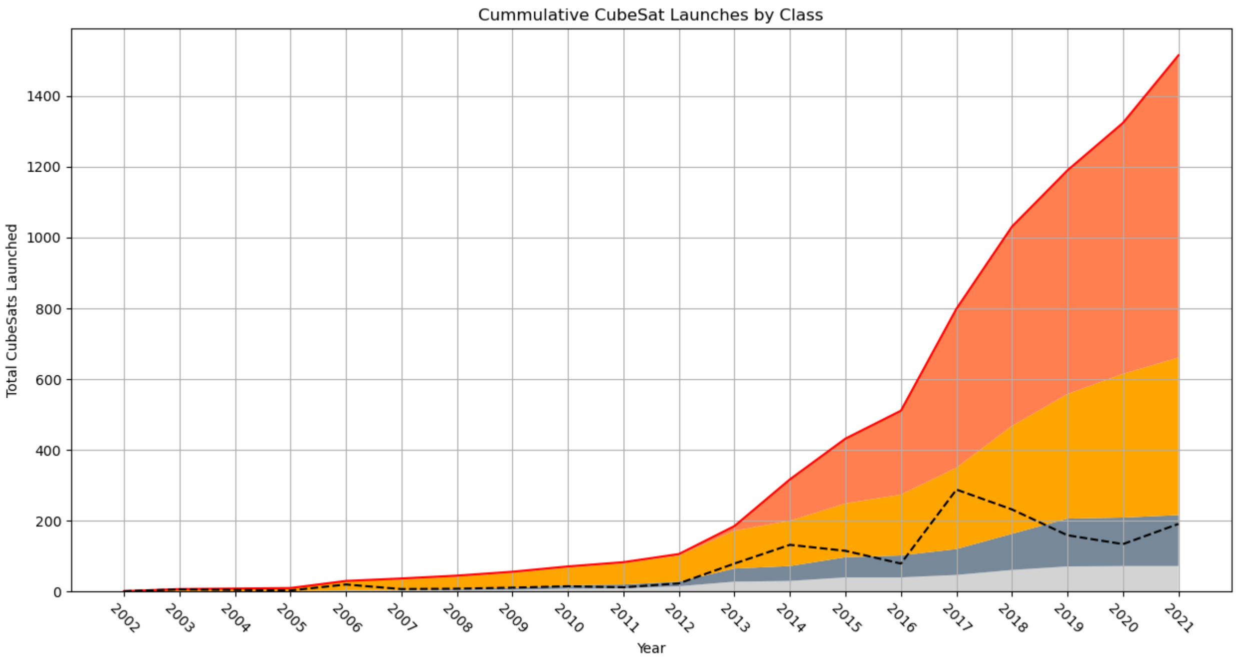

Figure 5.3: Cumulative CubeSats launched per year in four different classes — Military (light grey), Civil (dark grey), University (orange) and Commercial (red). The total number of CubeSats launched per year is shown as dashed black line — the impact of the COVID-10 pandemic on launch rates may be visible in the reduced launch rate in 2019/2020. More than 1500 CubeSats have been launched, allowing some statistical insights into their survival rates to be possible. Despite university launches initially dominating the total number of CubeSats, the most populous category is now commercial CubeSats such as Planet's 3U Dove satellites. Graph created with data from the CGEE CubeSat database [69], which contains launches up to April 29th 2021.

Figure 5.4 shows the current status of CubeSats launched since 2002. The data shows that older CubeSats are predominantly non-operational or deorbited, whereas CubeSats from more recent launches tend to be active. This suggests that CubeSats are becoming more reliable over time. However, it is difficult to estimate the typical lifetime of a CubeSat — as they have predominantly been deployed in Low Earth Orbit to date,

[2] Available at: https://www.cgee.org.br/web/observatorio-espacial/bancos-de-dados

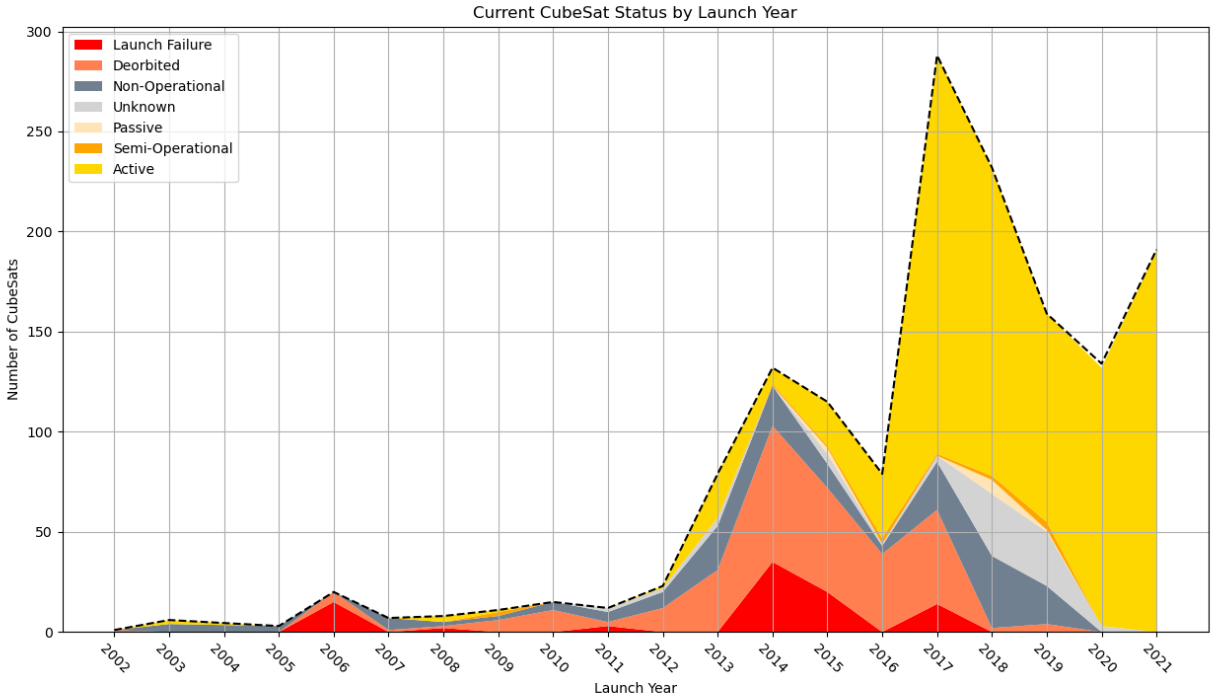

Figure 5.4: The graph shows the current status of CubeSats launched since 2002. The majority of CubeSats launched in 2002-2012 are either Non-operational, deorbited, or suffered launch failures. More recent launches tend to result in active satellites. A reasonable proportion of CubeSats (see Figure 5.5) are non-operational, passive, semi-operational, or have an unknown status — potentially causing problems with space sustainability. Graph created with data from the CGEE CubeSat database [69], which is accurate as of April 2021.

CubeSat lifetimes are determined by orbital decay in addition to subsystem failures [71]. The data does allow us to draw some conclusions, however; despite the improvements in technology and the cleaning affects of aerodynamic drag, 18.1% of CubeSats launched remain in orbit in either a non-operational, passive, semi-operational, or unknown state, as shown in Figure 5.5. We can use this as an upper bound on the proportion of swarm satellites we expect to be in a non-operational or degraded state, again operating under the assumption that CubeSats are a good model for swarm satellites.

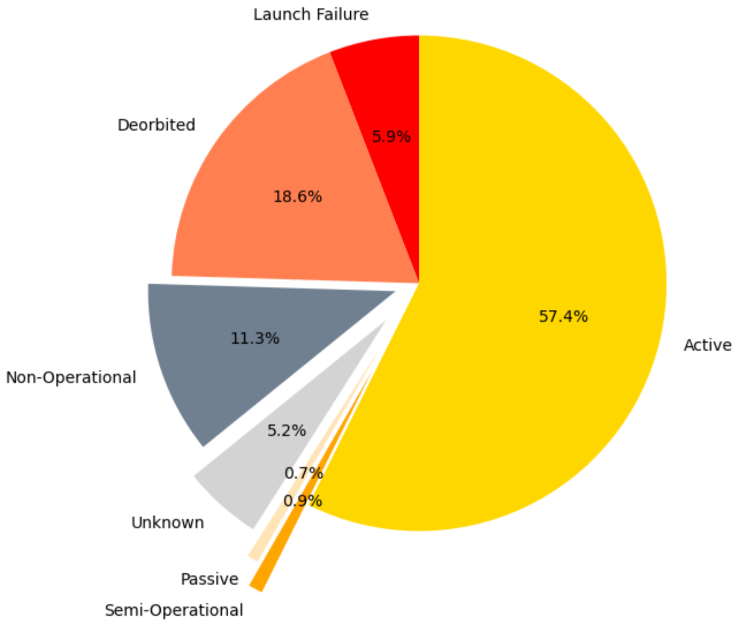

Figure 5.5: Pie Chart showing the current statues of CubeSats launched since 2002. Roughly a quarter of launched CubeSats either never made it to orbit of have been deorbited, and the majority of launched CubeSats (57.4%) are still active. However, 18.1% of CubeSats potentially pose a threat to space sustainability, and are indicated in the exploded sections in the figure. Graph created with data from the CGEE CubeSat database [69], which is accurate as of April 2021.

5.4 Next Steps

It is too early in this project to draw firm conclusions about the Satellite Health Indicator, but we are actively researching the two projects described in Section 5.3 and have identified next steps in this research beyond concluding those two investigations. With the Markov model defined and a upper bound of 18.1% of swarm satellites expected to be in a degraded state, we can start to weight the parameters of the satellite health indicator by the frequency with which subsystem failures lead to degraded states in the Markov model.

With that achieved, we will define a way to map real satellite telemetry to an estimate of the "health" of individual satellite subsystems. There is already published research using machine learning to analyse satellite telemetry [72] [73] as well as an open-source Python library designed to analyse satellite telemetry using machine learning algorithms [3].

Another route of investigation is to undertake a more rigorous investigation of satellite failures focusing on subsystems rather than entire satellites. The analysis of the CGEE CubeSat database provides a useful order-of-magnitude estimate for the number of swarm satellites we can expect to fail, but to constrain the weights of the satellite health indicator requires more fine-grained data, such as lists of satellite failures which focus on subsystems such as [64].

Finally, once these topics have been explored, it will be possible to compare the performance of different formulations of the satellite health indicator on sample satellite telemetry to find an optimal weighting to represent swarm satellite health. With this achieved we will be able to implement distributed estimation algorithms in a modelled satellite swarm and investigate if autonomous health monitoring can improve the longevity and sustainability of satellite swarms.

[3] Available at https://polarisml.space/

Chapter 6

Conclusions and Reflections

6.1 Conclusions

Ensuring that satellite swarms are deployed sustainably is an important field of research, and both the projects presented here represent steps towards sustainable swarms. The results of our research on cooperative localisation in satellite swarms indicates that the locations of a large swarm such as Starlink can be determined from inter-satellite measurements to an average RMSE of approximately 10.15 metres over most of their orbit, which could improve space situational awareness and provide a redundant way to localise swarm satellites in orbit. The results also show that inter-satellite cooperative localisation is dependent on the characteristics of the swarm geometry and the characteristics of inter-satellite links, which could inform the design of future satellite swarms.

The ongoing work on autonomous satellite heath monitoring could pave the way to predicting and preempting swarm satellite failures, but the analysis of CubeSat failures indicates that a small proportion of swarm satellites will still cause problems with space sustainability and debris creation. Ultimately, it may not be possible to render satellite swarms entirely sustainable, but these two projects outline research which could help upcoming satellite swarms be designed with sustainability in mind.

6.2 Personal Reflections

The original focus of this thesis was solely the autonomous health monitoring concept presented in Chapter 5. The summer project I had previously completed with Dr. Rajan was entitled "End-of-Life for Satellite Swarms", and this was the working title of this thesis. However, my discussions with co-workers at CAS and the steady stream of seminars at TU Delft led to me exploring an unexpected line of research — cooperative localisation in Starlink. I am deeply grateful to Dr. Rajan for encouraging me in this line of investigation and for supporting my academic curiosity.

As well as broadening the horizons of my research internship, working within CAS was occasionally challenging. As a research group focusing on the theory and applications of signal-processing, the research of other members of CAS was largely outwith my academic expertise, and I often encountered unfamiliar topics or methodologies. On the other hand, however, my experiences at CAS have left me comfortable with a wider range of topics and more skilled in aspects of programming, linear algebra, and data science.

This internship also gave me the opportunity to develop my understanding of space sustainability — during my time at TU Delft I was able to attend the 3rd Summit for Space Sustainability organised by the Secure World Foundation and the Space, Satellites, and Sustainability conference organised by SPIE in Glasgow, Scotland. On a more personal level, researching at TU Delft gave me the opportunity to live in the Netherlands and experience Dutch academic culture.

In summary, this internship has exposed me to new engineering topics as well as given me greater insight into the diversity of research currently underway in space sustainability, and I feel well prepared to pursue further research or a career in this field.

Bibliography

[1] Astropy Collaboration, T. P. Robitaille, E. J. Tollerud, P. Greenfield, *et al.*, "Astropy: A community Python package for astronomy," *Astronomy and Astrophysics*, vol. 558, A33, A33, Oct. 2013. DOI: 10.1051/0004-6361/201322068. arXiv: 1307.6212 [astro-ph.IM].

[2] Astropy Collaboration, A. M. Price-Whelan, B. M. Sipőcz, H. M. Günther, *et al.*, "The Astropy Project: Building an Open-science Project and Status of the v2.0 Core Package," *Astrophysical Journal*, vol. 156, no. 3, 123, p. 123, Sep. 2018. DOI: 10.3847/1538-3881/aabc4f. arXiv: 1801.02634 [astro-ph.IM].

[3] J. L. C. Rodríguez, J. M.G., A. Hidalgo, S. Bapat, *et al.*, *poliastro/poliastro: poliastro 0.15.2 (astroquery edition)*, version v0.15.2, Jun. 2021. DOI: 10.5281/zenodo.5035326.

[4] C. Turner and R. T. Rajan, "End-of-life for satellite swarms," in *71st International Astronautical Congress*, ser. 71, International Astronautical Federation, Sep. 2020.

[5] D. Selva, A. Golkar, O. Korobova, I. L. i. Cruz, *et al.*, "Distributed Earth Satellite Systems: What Is Needed to Move Forward?" *Journal of Aerospace Information Systems*, vol. 14, no. 8, pp. 412–438, 2017, Publisher: American Institute of Aeronautics and Astronautics _eprint: https://doi.org/10.2514/1.I010497. DOI: 10.2514/1.I010497.

[6] R. T. Rajan, S. Ben-Maor, S. Kaderali, C. Turner, *et al.*, "Applications and potentials of intelligent swarms (apis) for magnetospheric studies," in *71st International Astronautical Congress*, ser. 71, International Astronautical Federation, Sep. 2020.

[7] R. T. Rajan, S. Ben-Maor, S. Kaderali, C. Turner, *et al.*, "Applications and Potentials of Intelligent Swarms for magnetospheric studies," en, *Acta Astronautica*, Aug. 2021. DOI: 10.1016/j.actaastro.2021.07.046.

[8] E. Bonabeau, G. Theraulaz, J.-L. Deneubourg, S. Aron, *et al.*, "Self-organization in social insects," *Trends in Ecology & Evolution*, vol. 12, no. 5, pp. 188–193, May 1997. DOI: 10.1016/S0169-5347(97)01048-3.

[9] M. Ballerini, N. Cabibbo, R. Candelier, A. Cavagna, *et al.*, "Interaction ruling animal collective behavior depends on topological rather than metric distance: Evidence from a field study," *Proceedings of the National Academy of Sciences*, vol. 105, no. 4, pp. 1232–1237, Jan. 2008, Publisher: National Academy of Sciences Section: Biological Sciences. DOI: 10.1073/pnas.0711437105.

[10] S. Nag and L. Summerer, "Behaviour based, autonomous and distributed scatter manoeuvres for satellite swarms," *Acta Astronautica*, 6th International Workshop on Satellite Constellation and Formation Flying, vol. 82, no. 1, pp. 95–109, Jan. 2013. DOI: 10.1016/j.actaastro.2012.04.030.

[11] S. Jähnichen, K. Briess, and R. Burmeister, "Flying Sensors – Swarms in Space," in *Autonomous Systems – Self-Organization, Management, and Control*, B. Mahr and S. Huanye, Eds., Dordrecht: Springer Netherlands, 2008, pp. 71–77. DOI: 10.1007/978-1-4020-8889-6_8.

[12] C. Rouff, W. Truszkowski, J. Rash, and M. Hinchey, "Formal approaches to intelligent swarms," in *28th Annual NASA Goddard Software Engineering Workshop, 2003. Proceedings.*, Dec. 2003, pp. 51–57. DOI: 10.1109/SEW.2003.1270725.

[13] C. J. M. Verhoeven, M. J. Bentum, G. L. E. Monna, J. Rotteveel, *et al.*, "On the origin of satellite swarms," *Acta Astronautica*, vol. 68, no. 7, pp. 1392–1395, Apr. 2011. DOI: 10.1016/j.actaastro.2010.10.002.

[14] S. Engelen, C. J. M. Verhoeven, and M. J. Bentum, "Olfar, A Radio Telescope Based on Nano-Satellites in Moon Orbit," *Small Satellite Conference*, Aug. 2010.

[15] S. Curtis, W. Truszkowski, M. Rilee, and P. Clark, "ANTS for Human Exploration and Development of Space," in *2003 IEEE Aerospace Conference Proceedings (Cat. No.03TH8652)*, ISSN: 1095-323X, vol. 1, Mar. 2003, 1–261 vol.1. DOI: 10.1109/AERO.2003.1235057.

[16] H. Spence, K. Klein, J. Bookbinder, and H. Swarm, "The HelioSwarm Mission: A swarm of Small Satellites Revealing the Physics of Space Plasma Turbulence," *Small Satellite Conference*, Aug. 2019.

[17] H. Sanchez, D. Mcintosh, H. Cannon, C. Pires, *et al.*, "Starling1: Swarm Technology Demonstration," *Small Satellite Conference*, Aug. 2018.

[18] D. J. Kessler and B. G. Cour-Palais, "Collision frequency of artificial satellites: The creation of a debris belt," *Journal of Geophysical Research: Space Physics*, vol. 83, no. A6, pp. 2637–2646, 1978, _eprint: https://agupubs.onlinelibrary.wiley.com/doi/pdf/10.1029/JA083iA06p02637. DOI: https://doi.org/10.1029/JA083iA06p02637.

[19] C. J. Newman and M. Williamson, "Space Sustainability: Reframing the Debate," *Space Policy*, vol. 46, pp. 30–37, Nov. 2018. DOI: 10.1016/j.spacepol.2018.03.001.

[20] G. Brachet, "Protecting our space interests - Room: The Space Journal," en-US, *Room, The Space Journal*, vol. 10, no. 4, Dec. 2016.

[21] M. Palmroth, J. Tapio, A. Soucek, A. Perrels, *et al.*, "Toward Sustainable Use of Space: Economic, Technological, and Legal Perspectives," *Space Policy*, vol. 57, p. 101 428, Aug. 2021. DOI: 10.1016/j.spacepol.2021.101428.

[22] C. Pardini and L. Anselmo, "Assessment of the consequences of the Fengyun-1C breakup in low Earth orbit," *Advances in Space Research*, vol. 44, no. 5, pp. 545–557, Sep. 2009. DOI: 10.1016/j.asr.2009.04.014.

[23] S. Frey and S. Lemmens, "Status of the Space Environment: Current Level of Adherence to the Space Debris Mitigation Policy," in *7^{th} European Conference on Space Debris*, ESA Space Debris Office, 2017.

[24] European Space Agency. (2021). "Space debris by the numbers," [Online]. Available: https://www.esa.int/Safety_Security/Space_Debris/Space_debris_by_the_numbers (visited on 05/24/2021).

[25] United Nations Office for Outer Space Affairs, *Space Debris Mitigation Guidelines of the Committee on the Peaceful Uses of Outer Space*. Jan. 2018, Publisher: United Nations. DOI: 10.18356/2d85575e-en.

[26] H. Krag, F. Letizia, and S. Lemmens, "Space traffic management through the control of the space environment's capacity," *5th Eur. Work. Sp. Debris Model. Remediat. CNES HQ, Paris*, 2018.

[27] P. Guardabasso, M. P. Savino, C. Turner, R. Valeriani, *et al.*, "The recycler: An innovative approach to on-orbit servicing and repurposing," in *71^{st} International Astronautical Congress*, ser. 71, International Astronautical Federation, Sep. 2020.

[28] N. H. Barbara, S. Lizy-Destrez, P. Guardabasso, and D. Alary, "New GEO paradigm: Re-purposing satellite components from the geo graveyard," *Acta Astronautica*, vol. 173, pp. 155–163, 2020.

[29] R. Biesbroek, S. Aziz, A. Wolahan, S. Cipolla, *et al.*, "The clearspace-1 mission: Esa and clearspace team up to remove debris," in *Proc. 8th Eur. Conf. Sp. Debris*, 2021, pp. 1–3.

[30] Z. Serfontein, J. Kingston, S. Hobbs, I. E. Holbrough, *et al.*, "Drag augmentation systems for space debris mitigation," *Acta Astronautica*, 2021.

[31] M. Rathnasabapathy, F. Letizia, L. Stijn, M. Jah, *et al.*, "Space Sustainability Rating: Designing a Composite Indicator to Incentivise Satellite Operators to Pursue Long-Term Sustainability of the Space Environment," Online: rnational Astronautical Federation (IAF)., Oct. 2020.

[32] M. Jah and The University of Texas at Austin. (2017). "Astriagraph," [Online]. Available: http://astria.tacc.utexas.edu/AstriaGraph/ (visited on 05/14/2021).

[33] N. Simone, K. Nagpal, A. Gupta, M. Esteva, *et al.*, "Transparency and Accountability in Space Domain Awareness: Demonstrating ASTRIAGraph's Capabilities with the United Nations Registry Data," Jan. 2021, Accepted: 2021-02-25T16:27:56Z. DOI: 10.26153/tsw/11754.

[34] R. Walker, C. E. Martin, P. H. Stokes, and H. Klinkrad, "Sensitivity of long-term orbital debris environment evolution to the deployment of nano-satellite swarms," *Acta Astronautica*, vol. 51, no. 1, pp. 439–449, Jul. 2002. DOI: 10.1016/S0094-5765(02)00095-4.

[35] ESA. (2021). "ESA spacecraft dodges large constellation." En, [Online]. Available: https://www.esa.int/Safety_Security/ESA_spacecraft_dodges_large_constellation (visited on 11/13/2021).

[36] O. R. Hainaut and A. P. Williams, "Impact of satellite constellations on astronomical observations with ESO telescopes in the visible and infrared domains," En, *Astronomy & Astrophysics*, vol. 636, A121, Apr. 2020, Publisher: EDP Sciences. DOI: 10.1051/0004-6361/202037501.

[37] N. Patwari, J. Ash, S. Kyperountas, A. Hero, *et al.*, "Locating the nodes: Cooperative localization in wireless sensor networks," *IEEE Signal Processing Magazine*, vol. 22, no. 4, pp. 54–69, Jul. 2005, Conference Name: IEEE Signal Processing Magazine. DOI: 10.1109/MSP.2005.1458287.

[38] H. Wymeersch, J. Lien, and M. Z. Win, "Cooperative Localization in Wireless Networks," *Proceedings of the IEEE*, vol. 97, no. 2, pp. 427–450, Feb. 2009, Conference Name: Proceedings of the IEEE. DOI: 10.1109/JPROC.2008.2008853.

[39] Y. Gao, B. Xu, and L. Zhang, "Feasibility study of autonomous orbit determination using only the crosslink range measurement for a combined navigation constellation," *Chinese Journal of Aeronautics*, vol. 27, no. 5, pp. 1199–1210, 2014. DOI: https://doi.org/10.1016/j.cja.2014.09.005.

[40] P. K. Davé and K. Cahoy, "Autonomous satellite navigation using intersatellite laser communications," en, *Advances in the Astronautical Sciences*, vol. 171, 2020, Accepted: 2021-11-03T18:24:38Z.

[41] P. K. Dave, "Autonomous navigation of distributed spacecraft using intersatellite laser communications," Ph.D. dissertation, Massachusetts Institute of Technology, 2020.

[42] R. T. Rajan and A.-J. van der Veen, "Joint Ranging and Synchronization for an Anchorless Network of Mobile Nodes," *IEEE Transactions on Signal Processing*, vol. 63, no. 8, pp. 1925–1940, Apr. 2015, Conference Name: IEEE Transactions on Signal Processing. DOI: 10.1109/TSP.2015.2391076.

[43] S. Kay, *Fundamentals of statistical signal processing — Guide books*, En.

[44] H. L. V. Trees, *Detection, Estimation, and Modulation Theory, Part I: Detection, Estimation, and Linear Modulation Theory*, en. John Wiley & Sons, Apr. 2004.

[45] N. Patwari, A. Hero, M. Perkins, N. Correal, *et al.*, "Relative location estimation in wireless sensor networks," *IEEE Transactions on Signal Processing*, vol. 51, no. 8, pp. 2137–2148, Aug. 2003, Conference Name: IEEE Transactions on Signal Processing. DOI: 10.1109/TSP.2003.814469.

[46] D. Bhattacherjee and A. Singla, "Network topology design at 27,000 km/hour," in *Proceedings of the 15th International Conference on Emerging Networking Experiments And Technologies*, ser. CoNEXT '19, New York, NY, USA: Association for Computing Machinery, Dec. 2019, pp. 341–354. DOI: 10.1145/3359989.3365407.

[47] A. C. Boley and M. Byers, "Satellite mega-constellations create risks in Low Earth Orbit, the atmosphere and on Earth," en, *Scientific Reports*, vol. 11, no. 1, p. 10 642, May 2021. DOI: 10.1038/s41598-021-89909-7.

[48] V. L. Foreman, A. Siddiqi, and O. D. Weck, "Large Satellite Constellation Orbital Debris Impacts: Case Studies of OneWeb and SpaceX Proposals," in *AIAA SPACE and Astronautics Forum and Exposition*, _eprint: https://arc.aiaa.org/doi/pdf/10.2514/6.2017-5200, American Institute of Aeronautics and Astronautics. DOI: 10.2514/6.2017-5200.

[49] J. C. McDowell, "The Low Earth Orbit Satellite Population and Impacts of the SpaceX Starlink Constellation," en, *The Astrophysical Journal*, vol. 892, no. 2, p. L36, Apr. 2020, Publisher: American Astronomical Society. DOI: 10.3847/2041-8213/ab8016.

[50] A. U. Chaudhry and H. Yanikomeroglu, "Laser Intersatellite Links in a Starlink Constellation: A Classification and Analysis," *IEEE Vehicular Technology Magazine*, vol. 16, no. 2, pp. 48–56, Jun. 2021, Conference Name: IEEE Vehicular Technology Magazine. DOI: 10.1109/MVT.2021.3063706.

[51] O. B. Osoro and E. J. Oughton, "A Techno-Economic Framework for Satellite Networks Applied to Low Earth Orbit Constellations: Assessing Starlink, OneWeb and Kuiper," *IEEE Access*, vol. 9, pp. 141 611–141 625, 2021, Conference Name: IEEE Access. DOI: 10.1109/ACCESS.2021.3119634.

[52] C. Turner, "Simulated Megaconstellation Ephemerides," En, Jul. 2021, Publisher: IEEE Type: dataset.

[53] D. A. Vallado, *Fundamentals of astrodynamics and applications*. Springer Science & Business Media, 2001, vol. 12.

[54] G. H. Kaplan, "The IAU Resolutions on Astronomical Reference Systems, Time Scales, and Earth Rotation Models," *arXiv:astro-ph/0602086*, Feb. 2006, arXiv: astro-ph/0602086.

[55] Space Exploration Holdings, LLC, *Application for Fixed Satellite Service*, Apr. 2020.

[56] S. Cakaj, B. Kamo, V. Koliçi, and O. Shurdi, "The Range and Horizon Plane Simulation for Ground Stations of Low Earth Orbiting (LEO) Satellites," en, *International Journal of Communications, Network and System Sciences*, vol. 4, no. 9, pp. 585–589, Sep. 2011, Number: 9 Publisher: Scientific Research Publishing. DOI: 10.4236/ijcns.2011.49070.

[57] S. Cakaj and K. Malarić, "Rigorous analysis on performance of LEO satellite ground station in urban environment," en, *International Journal of Satellite Communications and Networking*, vol. 25, no. 6, pp. 619–643, 2007, _eprint: https://onlinelibrary.wiley.com/doi/pdf/10.1002/sat.895. DOI: 10.1002/sat.895.

[58] S. Cakaj, M. Fitzmaurice, J. Reich, and E. Foster, "Simulation of Local User Terminal Implementation for Low Earth Orbiting (LEO) Search and Rescue Satellites," in *2010 Second International Conference on Advances in Satellite and Space Communications*, Jun. 2010, pp. 140–145. DOI: 10.1109/SPACOMM.2010.9.

[59] S. Cakaj, "The Parameters Comparison of the "Starlink" LEO Satellites Constellation for Different Orbital Shells," *Frontiers in Communications and Networks*, vol. 2, p. 7, 2021. DOI: 10.3389/frcmn.2021.643095.

[60] I. del Portillo, B. G. Cameron, and E. F. Crawley, "A technical comparison of three low earth orbit satellite constellation systems to provide global broadband," en, *Acta Astronautica*, vol. 159, pp. 123–135, Jun. 2019. DOI: 10.1016/j.actaastro.2019.03.040.

[61] P. Zhou, B. W. Ang, and K. L. Poh, "A mathematical programming approach to constructing composite indicators," en, *Ecological Economics*, Special Section: Ecological-economic modelling for designing and evaluating biodiversity conservation policies, vol. 62, no. 2, pp. 291–297, Apr. 2007. DOI: 10.1016/j.ecolecon.2006.12.020.

[62] S. M. Hatefi and S. A. Torabi, "A common weight MCDA–DEA approach to construct composite indicators," en, *Ecological Economics*, vol. 70, no. 1, pp. 114–120, Nov. 2010. DOI: 10.1016/j.ecolecon.2010.08.014.

[63] Y. Ding, Y. Fu, K. K. Lai, and W. K. John Leung, "Using Ranked Weights and Acceptability Analysis to Construct Composite Indicators: A Case Study of Regional Sustainable Society Index," En, *Social Indicators Research*, vol. 139, no. 3, pp. 871–885, Oct. 2018. DOI: 10.1007/s11205-017-1765-3.

[64] R. A. Haga and J. H. Saleh, "Epidemiology of satellite anomalies and failures: A subsystem-centric approach," in *2011 Aerospace Conference*, ISSN: 1095-323X, Mar. 2011, pp. 1–19. DOI: 10.1109/AERO.2011.5747656.

[65] S. Engelen, E. Gill, and C. Verhoeven, "On the reliability, availability, and throughput of satellite swarms," *IEEE Transactions on Aerospace and Electronic Systems*, vol. 50, no. 2, pp. 1027–1037, Apr. 2014, Conference Name: IEEE Transactions on Aerospace and Electronic Systems. DOI: 10.1109/TAES.2014.120711.

[66] C. Chantal, B. Simone, and M. Benjamin K., *Cubesat Handbook*, en. Elsevier, 2021. DOI: 10.1016/C2018-0-02366-X.

[67] J.-F. Castet and J. H. Saleh, "Beyond reliability, multi-state failure analysis of satellite subsystems: A statistical approach," *Reliability Engineering & System Safety*, vol. 95, no. 4, pp. 311–322, 2010.

[68] J. Guo, L. Monas, and E. Gill, "Statistical analysis and modelling of small satellite reliability," en, *Acta Astronautica*, vol. 98, pp. 97–110, May 2014. DOI: 10.1016/j.actaastro.2014.01.018.

[69] T. Villela, C. A. Costa, A. M. Brandão, F. T. Bueno, *et al.*, "Towards the Thousandth CubeSat: A Statistical Overview," en, *International Journal of Aerospace Engineering*, vol. 2019, e5063145, Jan. 2019, Publisher: Hindawi. DOI: 10.1155/2019/5063145.

[70] M. Swartwout, "The first one hundred cubesats: A statistical look," *Journal of small Satellites*, vol. 2, no. 2, pp. 213–233, 2013.

[71] L. Qiao, C. Rizos, and A. G. Dempster, "Analysis and comparison of cubesat lifetime," in *Proceedings of the 12th Australian Space Conference*, Citeseer, 2013, pp. 249–260.

[72] S. K. Ibrahim, A. Ahmed, M. A. E. Zeidan, and I. E. Ziedan, "Machine Learning Methods for Spacecraft Telemetry Mining," *IEEE Transactions on Aerospace and Electronic Systems*, vol. 55, no. 4, pp. 1816–1827, Aug. 2019, Conference Name: IEEE Transactions on Aerospace and Electronic Systems. DOI: 10.1109/TAES.2018.2876586.

[73] C. OMeara, L. Schlag, and M. Wickler, "Applications of deep learning neural networks to satellite telemetry monitoring," in *2018 SpaceOps Conference*, 2018, p. 2558.

Appendices

Appendix A

Megaconstellation Ephemerides Data Format

Index		Identifiers			Classical Orbital Elements						Position			Velocity		
Satellite ID	**Time**	**Plane No.**	**Sat. No.**	**Time**	a	e	i	$RAAN$	$ArgP$	ν	$\vec{r}_x$	$\vec{r}_y$	$\vec{r}_z$	$\vec{v}_x$	$\vec{v}_y$	$\vec{v}_z$
s01001	0.0	1	1	0	6928	0	53°	0°	0°	0°	6928.0	0.0	0.0	0.0	4.56	6.06
s01001	10.0	1	1	10	6928	0	53°	0°	0°	0.63°	6927.58	45.65	60.58	-0.083	4.56	6.06
⋮	⋮	⋮	⋮	⋮	⋮	⋮	⋮	⋮	⋮	⋮	⋮	⋮	⋮	⋮	⋮	⋮
s01001	5730.0	1	1	5730	6928	0	53°	0°	0°	359.45 °	6927.68	-40.27	-53.44	0.07	4.56	6.06
s01002	0.0	1	2	0	6928	0	53°	0°	0°	16.36°	6647.37	1174.65	1558.81	-2.14	4.38	5.81
⋮	⋮	⋮	⋮	⋮	⋮	⋮	⋮	⋮	⋮	⋮	⋮	⋮	⋮	⋮	⋮	⋮
s01002	5730.0	1	2	5730	6928	0	53°	0°	0°	375.81 °	6665.91	1135.95	1507.46	-2.07	4.39	5.83
⋮	⋮	⋮	⋮	⋮	⋮	⋮	⋮	⋮	⋮	⋮	⋮	⋮	⋮	⋮	⋮	⋮
⋮	⋮	⋮	⋮	⋮	⋮	⋮	⋮	⋮	⋮	⋮	⋮	⋮	⋮	⋮	⋮	⋮
s01022	0.0	1	22	5730	6928	0.0	53	0.0°	0.0°	703.08°	6628.20	-1213.24	-1610.02	2.21	4.37	5.79
s02001	0.0	2	1	0	6928	0.0	53	5.0°	0.0°	0.0°	6901.64	603.81	0.0	-0.40	4.55	6.06
⋮	⋮	⋮	⋮	⋮	⋮	⋮	⋮	⋮	⋮	⋮	⋮	⋮	⋮	⋮	⋮	⋮
⋮	⋮	⋮	⋮	⋮	⋮	⋮	⋮	⋮	⋮	⋮	⋮	⋮	⋮	⋮	⋮	⋮
⋮	⋮	⋮	⋮	⋮	⋮	⋮	⋮	⋮	⋮	⋮	⋮	⋮	⋮	⋮	⋮	⋮
s72022	0.0	72	22	0	6928	0	53°	355.0°	0°	343.64°	6519.69	-1749.53	-1558.81	2.51	4.18	5.81
⋮	⋮	⋮	⋮	⋮	⋮	⋮	⋮	⋮	⋮	⋮	⋮	⋮	⋮	⋮	⋮	⋮
s72022	5730.0	72	22	5730	6928	0	53°	355.0°	0°	703.08°	6497.24	-1786.30	-1610.02	2.58	4.16	5.79

Figure A.1: Format of the ephemerides data created by the code described in Chapter 4.

Appendix B

CRLB Example Calculation

In this Appendix, a sample calculation is shown for the toy CRB problem described in Section 4.3. The set-up for the calculation is shown in Figure B.1, and shows the values used to calculate an entries in the $[\mathbf{F}_{xx}]$ Fisher submatrix for node number 15. In this example, only the value for TOA is considered. *"Locating the nodes"* by Patwari *et al.* (2005) [37] gives the requisite expressions:

$$[\mathbf{F}_{xx}]_{k,l} = \begin{cases} \gamma \sum_{i \in H(k)} (x_k - x_i)^2 / d_{k,i}^2 & k = l \\ -\gamma I_{H(k)}(l)(x_k - x_l)^2 / d_{k,l}^2 & k \neq l \end{cases} \tag{B.1}$$

where $\gamma_{TOA} = \frac{1}{(v_p \sigma_T)^2}$, $\sigma_T = 6.1$ ns and $v_p = 3.8 \cdot 10^8$ ms^{-1}. The other notation is explained in Chapter 5. For node 15, the set of connected nodes is $\{5, 9, 10, 11, 14, 16, 17, 19, 20\}$ as well as anchor number 4 ($A4$). To calculate the matrix entry $[\mathbf{F}_{xx}]_{15,15}$ we use the following formula:

$$[\mathbf{F}_{xx}]_{15,15} = \gamma \sum_{i \in H(k)} (x_k - x_i)^2 / d_{k,i}^2 \tag{B.2}$$

Considering the set-up shown in Figure B.1 gives:

$$\begin{aligned} [\mathbf{F}_{xx}]_{15,15} = \gamma \Bigg[&\frac{(x_{15} - x_5)^2}{d_{15,5}^2} + \frac{(x_{15} - x_9)^2}{d_{15,9}^2} + \frac{(x_{15} - x_{10})^2}{d_{15,10}^2} + \frac{(x_{15} - x_{11})^2}{d_{15,11}^2} + \frac{(x_{15} - x_{14})^2}{d_{15,14}^2} \\ &+ \frac{(x_{15} - x_{16})^2}{d_{15,16}^2} + \frac{(x_{15} - x_{17})^2}{d_{15,17}^2} + \frac{(x_{15} - x_{19})^2}{d_{15,19}^2} + \frac{(x_{15} - x_{20})^2}{d_{15,20}^2} + \frac{(x_{15} - x_{A4})^2}{d_{15,A4}^2} \Bigg] \end{aligned} \tag{B.3}$$

Plugging in the values gives the following equation:

$$[\mathbf{F}_{xx}]_{15,15} = 0.2799 \left[\frac{0.0^2}{10.0^2} + \frac{-5.0^2}{7.07^2} + \frac{0.0^2}{5.0^2} + \frac{5.0^2}{7.07^2} + \frac{-5.0^2}{5.0^2} + \frac{5.0^2}{5.0^2} + \frac{10.0^2}{10.0^2} + \frac{0.0^2}{5.0^2} + \frac{5.0^2}{7.07^2} + \frac{-5.0^2}{7.07^2} \right] = 1.493 \tag{B.4}$$

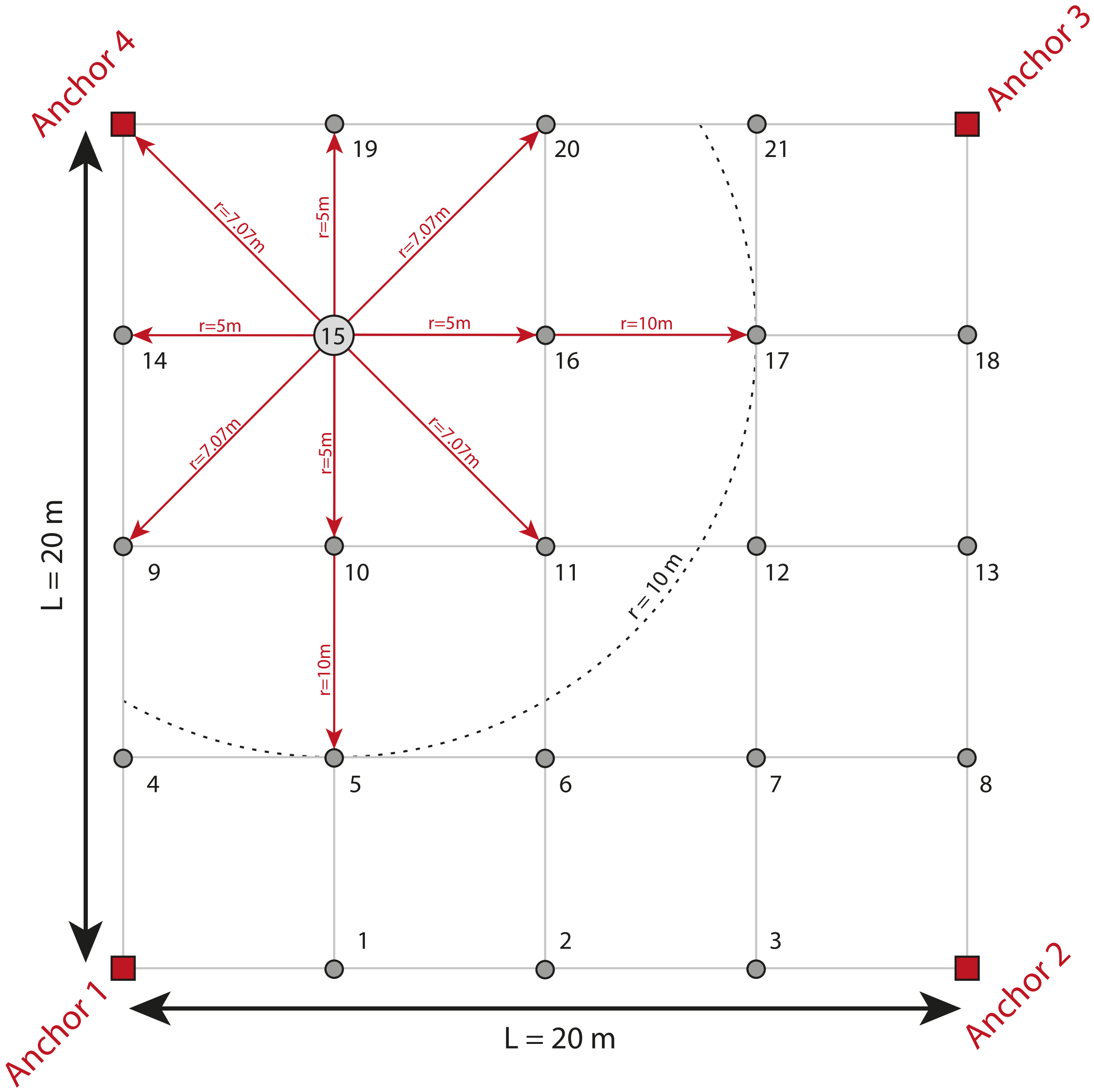

Figure B.1: Set-up for the Example Calculation of the CRLB based on Patwari *et al.*

Appendix C

Starlink Ground Stations

C.1 Active Ground Stations

This section lists the location of active Starlink ground stations, which at the time of writing are all located in the USA [1]. All ground stations were verified against an FCC filing.

Planned Ground Stations — USA				
Name	**Region**	**Latitude**	**Longitude**	**Source**
Kuparuk	Alaska	70.4244° N	148.8708° W	FCC Filing
Charleston	Oregon	43.3401° N	124.3301° W	FCC Filing
Redmond	Washington	47.6740° N	122.1215° W	FCC Filing
Kalama	Washington	46.0084° N	122.8446° W	FCC Filing
Tionesta	Califonia	41.6487° N	121.2906° W	FCC Filing
Arbuckle	Califonia	39.0174° N	122.0577° W	FCC Filing
Robbins	Califonia	38.8703° N	121.7052° W	FCC Filing
Los Angeles	Califonia	34.0522° N	118.2437° W	FCC Filing
Hawthorne	Califonia	33.9164° N	118.3526° W	FCC Filing
Roll	Arizona	32.7517° N	113.9891° W	FCC Filing
Panaca	Nevada	37.7891° N	114.3847° W	FCC Filing
Vernon	Utah	40.0922° N	112.4336° W	FCC Filing
Evanston	Wyoming	41.2683° N	110.9632° W	FCC Filing
Butte	Montana	46.0038° N	112.5348° W	FCC Filing
Colburn	Idaho	48.3971° N	116.5352° W	FCC Filing
Conrad	Montana	48.1683° N	111.9447° W	FCC Filing
Slope County	North Dakota	46.4129° N	103.5021° W	FCC Filing
Inman	Kansas	38.2320° N	97.7734° W	FCC Filing
Nemaha	Nebraska	40.3383° N	95.6730° W	FCC Filing
Dumas	Texas	35.8654° N	101.9732° W	FCC Filing
Springer	OK	34.3145° N	97.1428° W	FCC Filing
McGregor	Texas	31.4441° N	97.4092° W	FCC Filing

[1] According to Starlink Gateways

Sanderson	Texas	30.1424° N	102.3940° W	FCC Filing
Boca Chica	Texas	25.9920° N	97.1822° W	FCC Filing
Hamshire	Texas	29.8599° N	94.3093° W	FCC Filing
Warren	Missouri	38.8212° N	91.1392° W	FCC Filing
Robertsdale	Alabama	30.5538° N	87.7119° W	FCC Filing
Merrillan	Wisconsin	44.4511° N	90.8413° W	FCC Filing
Marcell	Minesota	47.5930° N	93.6908° W	FCC Filing
Hitterdal	Minesota	46.9775° N	96.2592° W	FCC Filing
Cass County	Minesota	47.2145° N	94.2309° W	FCC Filing
Punta Gorda	Forida	26.9298° N	82.0454° W	FCC Filing
Baxley	Georgia	31.7783° N	82.3485° W	FCC Filing
Tracy City	Tennessee	35.2604° N	85.7361° W	FCC Filing
Gaffney	South Carlina	35.0718° N	81.6498° W	FCC Filing
Mandale	North Carolina	35.8532° N	79.2731° W	FCC Filing
Wise	North Carolina	36.4865° N	78.1708° W	FCC Filing
Greenville	Pennsylvania	41.4045° N	80.3912° W	FCC Filing
Lockport	New York	43.1706° N	78.6903° W	FCC Filing
Litchfield	Connecticut	41.7473° N	73.1887° W	FCC Filing
Beekmantown	New York	44.7709° N	73.4921° W	FCC Filing
Lunenburg	Vermont	44.4631° N	71.6820° W	FCC Filing
Sullivan	Maine	44.5265° N	68.1518° W	FCC Filing
Loring	Maine	46.9086° N	67.8258° W	FCC Filing
Hillman	Michigan	45.0592° N	83.9011° W	FCC Filing
Manistique	Michigan	45.9578° N	86.2463° W	FCC Filing
Prosser	Washington	46.2068° N	119.7689° W	FCC Filing

Table C.1: Active Starlink Ground Station locations in the USA based on filings with the Federal Communications Commission. All latitudes and longitudes are approximate.

C.2 Planned Ground Stations

In this section, the names and locations of planned Starlink ground stations is shown based on regulatory filings in the USA (Table C.2), Chile (Table C.3), France (Table C.4), UK (Table C.5), Australia (Table C.6), and New Zealand (Table C.7). Planned or experimental ground stations have also been reported in Canada, Ireland, Germany, Poland, and Turkey but as official filings are not publicly available (and therefore not verifiable) they are omitted here [2].

[2] See for example Starlink Gateways and Starlink Coverage Tracker.

Planned Ground Stations — USA				
Name	**Region**	**Latitude**	**Longitude**	**Source**
Nome	Alaska	64.5011° N	165.4064° W	FCC Filing
Fairbanks	Alaska	64.8378° N	147.7164° W	FCC Filing
Ketchikan	Alaska	55.3422° N	131.6461° W	FCC Filing
Rolette	North Dakota	48.6608° N	99.8415° W	FCC Filing
Broadview	Illinois	41.8639° N	87.8534° W	FCC Filing
Lawrence	Kansas	38.9717° N	95.2353° W	FCC Filing
Norcoss	Georgia	33.9411° N	84.2137° W	FCC Filing
New Braunfels	Texas	29.7030° N	98.1245° W	FCC Filing
Kenansville	Florida	27.8765° N	80.9883° W	FCC Filing
Fort Lauderdale	Florida	26.1224° N	80.1373° W	FCC Filing

Table C.2: Planned Starlink Ground Station locations in the USA based on filings with the Federal Communications Commission. All latitudes and longitudes are approximate.

Planned Ground Stations — Chile				
Name	**Region**	**Latitude**	**Longitude**	**Source**
Punta Arenas	De Magallanes y de la Antártica Chilena	53.1638° S	70.9171° W	MTT Filing
Pudahuel	Metropolitana de Santiago	33.4421° S	70.7641° W	MTT Filing
Caldera	De Atacama	27.0667°S	70.8178° W	MTT Filing
Coquimbo	De Coquimbo	29.9590° S	71.3389° W	MTT Filing
Talca	Del Maule	35.4232° S	71.6485° W	MTT Filing
Puerto Saavedra	De La Araucanía	38.7837° S	73.3987° W	MTT Filing
Puerto Montt	De Los Lagos	41.4689° S	72.9411° W	MTT Filing

Table C.3: Planned Starlink Ground Station locations in Chile based on filings with the República De Chile Ministerio De Transportes Y Telecomunicaciones Subsecretaría De Telecomunicaciones. All latitudes and longitudes are approximate.

Planned Ground Stations — France				
Name	**Region**	**Latitude**	**Longitude**	**Source**
Villenave d'Ornon	Gironde	44.7800° N	0.5673° W	ARCEP Filing
Gravelines	Nord	50.9871° N	2.1255° E	ARCEP Filing

Table C.4: Planned Starlink Ground Station locations in France based on filings with the Autorité de Régulation des Communications Électroniques et des Postes. All latitudes and longitudes are approximate.

Planned Ground Stations — UK				
Name	**Region**	**Latitude**	**Longitude**	**Source**
Douglas	Isle of Man	54.1523° N	4.4861° W	Ofcom Filing
Goonhilly	Cornwall	50.0500° N	5.2000° W	Ofcom Filing
Chalfont Grove	Buckinghamshire	51.6150° N	0.5727° W	Ofcom Filing

Table C.5: Planned Starlink Ground Station locations in the United Kingdom based on filings with the Office of Communications. All latitudes and longitudes are approximate.

Planned Ground Stations — Australia				
Name	**Region**	**Latitude**	**Longitude**	**Source**
Bogantungan	Queensland	23.6463° S	147.2926° E	ACMA Filing
Calrossie	New South Wales	29.05778° S	150.0400° E	ACMA Filing
Cataby	Western Australia	30.7358° S	115.5402° E	ACMA Filing
Wagin	Western Australia	33.3050° S	117.3444° E	ACMA Filing
Merredin	Western Australia	31.4832° S	118.2833° E	ACMA Filing
Bullabulling	Western Australia	31.0133° S	120.8669° E	ACMA Filing
Pimba	South Australia	31.2537° S	136.8001° E	ACMA Filing
Broken Hill	NSW	31.9596° S	141.4608° E	ACMA Filing
Springbrook Creek	New South Wales	30.4398° S	149.6838 ° E	ACMA Filing
Ki Ki	South Australia	35.5685° S	139.7939° E	ACMA Filing
Torrumbarry	Victoria	35.9761° S	144.4869° E	ACMA Filing
Cobargo	New South Wales	36.3866° S	149.9018° E	ACMA Filing

Table C.6: Planned Starlink Ground Station locations in Australia based on filings with the Australian Communications and Media Authority. All latitudes and longitudes are approximate.

Planned Ground Stations — New Zealand				
Name	**Region**	**Latitude**	**Longitude**	**Source**
Puwera	Northland	35.7962° S	174.2927° E	RSM Filing
Te Hana	Auckland	36.2556° S	174.5093° E	RSM Filing
Clevedon	Auckland	36.9914° S	175.0377° E	RSM Filing
Hinds	Mid-Canterbury	44.0021° S	171.5700° E	RSM Filing
Cromwell	Otago	45.0459° S	169.1956° E	RSM Filing
Awarua	Southland	46.4923° S	168.3808° E	RSM Filing

Table C.7: Planned Starlink Ground Station locations in New Zealand based on filings with the Ministry of Business, Innovation & Employment, Radio Spectrum Management. All latitudes and longitudes are approximate.